May 10, 2002

Annual Report for Contract NASW-00007

Experimental Simulations of Large-Scale Collisions

Period of performance: June 23, 2001 – June 22, 2002

Principal Investigator:	Kevin R. Housen
Institution:	The Boeing Co.
Address:	MS 2T-50
	P.O. Box 3999
City/State/Zip Code:	Seattle, WA 98124
Telephone:	(206) 544-5415
	(206) 544-5438 (FAX)
e-mail:	kevin.r.housen@boeing.com

Introduction

The densities of some 22 small bodies are now known, thanks mainly to recent improvements in ground-based observational techniques and data obtained in the Galileo and NEAR spacecraft missions. Nearly half of these objects have densities below 2.0 gm/cm^2, and about one-fourth have densities below 1.5 gm/cm^3 (Britt *et al.* 2002).

Estimates of the porosity of these bodies have been made by associating various taxonomic classes of asteroids with analogue classes of meteorites. The bulk porosity of an asteroid, i.e. the fraction of an asteroids volume that is void, is calculated from the known bulk density of the asteroid and the measured density of mineral grains in the corresponding analogue meteorite type. Such calculations show that many asteroids have significant pore space (Consolmagno and Britt 1998, Flynn *et al.* 1999, Wilson *et al.* 1999, Britt and Consolmagno 2000, Wilkison *et al.* 2001). For example, Britt *et al.* (2002) find porosities as high as 75%, with a clustering of objects in the range of 25-55%. These observations have made it clear that void space makes up a significant part of the interiors of many asteroids. Comets, too, are probably very porous. Greenberg (1986) and Sirono and Greenberg (2000) estimate that the porosity of comets is in the range of 60% to 80%.

The NEAR images of asteroid Mathilde illustrated the degree to which porosity affects the impact cratering process. The unusual characteristics of Mathilde's crater population cannot be readily explained using the classical picture of cratering that has developed over the past decades of laboratory impact research with conventional geological materials, such as dry soils or rock. Mathilde has a surprising abundance of relatively large craters on its surface. With only ~50% of the surface area observed, four of the craters have diameters exceeding Mathilde's mean radius of 26 km (Veverka *et al.*, 1997). These craters are noteworthy because they left both Mathilde and themselves intact (Chapman *et al.*, 1999; Thomas *et al.*, 1999). While single craters on other small bodies have been observed with about the same ratio of crater size to body size, the fact that Mathilde survived at least four large impacts is quite unusual.

Even more surprising is the fact that the large craters formed in close proximity with little mutual degradation from ejecta blanketing or seismic shaking. Laboratory measurements of ejecta for cratering in dry soils indicate that, even in Mathilde's weak gravity field, ejecta deposits near the rims of the large craters should be ~ 1 km deep, which should have had a noticeable effect on earlier craters. The fact that degradation did not occur has been attributed to Mathilde's low density of 1.3±0.2 gm/cm^3 (Veverka *et al.*, 1997), and high porosity of 50±20% (Veverka *et al.*, 1999).

If the tightly packed barren craters are a result of Mathilde's porosity, then other low-density bodies might be expected to show similar features. In fact, the recent discoveries of low-density C-like objects (e.g. Eugenia, 2000 DP107, and others) suggest that "unusual" craters may be the norm in the asteroid belt. The purpose of the research reported here is to gain a better understanding of the mechanics of cratering in porous materials. Such an understanding is necessary in order to decipher the information that asteroid observations contain regarding the collisional evolution of porous asteroids and satellites.

Ejecta from impacts into porous asteroids

We performed exploratory impact experiments in a highly porous, crushable, material that demonstrated a previously unrecognized mechanism of crater formation, and suggested that cratering events on porous asteroids may be substantially different from those on rocky objects (Housen *et al.*, 1999). The craters were found to form primarily by compaction of the target material, rather than the process of excavation that occurs in typical soils. A significant consequence of this compaction cratering is that very little material is excavated to form an ejecta blanket.

Most of the earlier work conducted under this research program has made use of a geotechnic centrifuge (Figure 1). Centrifuge experiments are useful because they allow one to simulate the formation of craters at scales much larger than otherwise attainable in the lab. The centrifuge simulation method is well-rooted both on a theoretical basis (e.g. Schmidt and Holsapple 1980, Holsapple and Schmidt, 1987) and by comparison with large-scale explosion testing (e.g. Schmidt 1978, Housen and Holsapple 2002).

It may seem odd to employ a centrifuge in the study of impacts on asteroids, where gravity fields are obviously quite weak. However, it is important to realize that, even with their meager gravity fields, the lithostatic stresses involved in the formation of, say, a 30-km diameter crater on a 100-km asteroid, are about 500 times larger than those for a 10-cm crater formed at 1G in the lab. To reproduce the lithostatic stresses of the asteroid crater[1], the small-scale experiment must be conducted at an acceleration of 500G. Equally important, material ejected during an impact experiment on the centrifuge will experience the same ballistics as the material in the simulated asteroid event. For this reason, centrifuge simulations provide the only experimental avenue to gain insights into large-scale cratering on asteroids.

Centrifuge experiments are conducted under a specific set of conditions such that the small-scale crater is *similar* to an asteroid crater[2]. The term similar here means that the experimental crater is a geometric replica of the larger crater. The length scale factor that relates the two craters is g_C/g_A, where g_C and g_A are the accelerations on the centrifuge and the asteroid, respectively (Housen and Holsapple, 2002). As an example, a 500-G simulation of an impact on Mathilde (where $g_A=10^{-3}$G) provides a length scale factor of 5×10^5. Therefore, Mathilde's largest crater (~30 km diameter) is simulated by a crater only 6 cm in diameter on the centrifuge. This experimental crater is similar in the sense that it is a geometric replica of the asteroid crater and because it reproduces the lithostatic stresses and ejecta ballistics of its asteroid counterpart.

The first centrifuge impact experiments using porous materials showed some remarkable results (Housen *et al.* 1999). Three experiments were conducted at 500G in a single target. The first impact formed a crater that had a normal bowl-like shape, but was unusual in that only a very small mass of ejecta was found around the crater, indicating

[1] This is crucial, because the shear strength of geological materials depends on the confining pressure

[2] The conditions for similarity are satisfied if the target and impactor materials and the impact velocity are the same for the experimental and asteroid craters (Housen and Holsapple, 2002).

that only a few percent of the mass originally contained within the crater was ejected. The second impact point was positioned in a way to leave a small distance between the rims of the two craters. Photographs and profile measurements of the first crater before and after the second impact showed that the second impact had no measurable effect on its predecessor. The third crater was formed such that its rim just intersected the rims of the first two craters, which resulted in some slumping of material into those craters. The target surface was essentially barren after all three impacts, suggesting only minimal ejection of material. These results showed that large craters in highly porous materials can form in very close proximity with very little degradation to earlier craters. Evidently the porous material causes extreme decay of the impact shock pressure and suppresses ejecta.

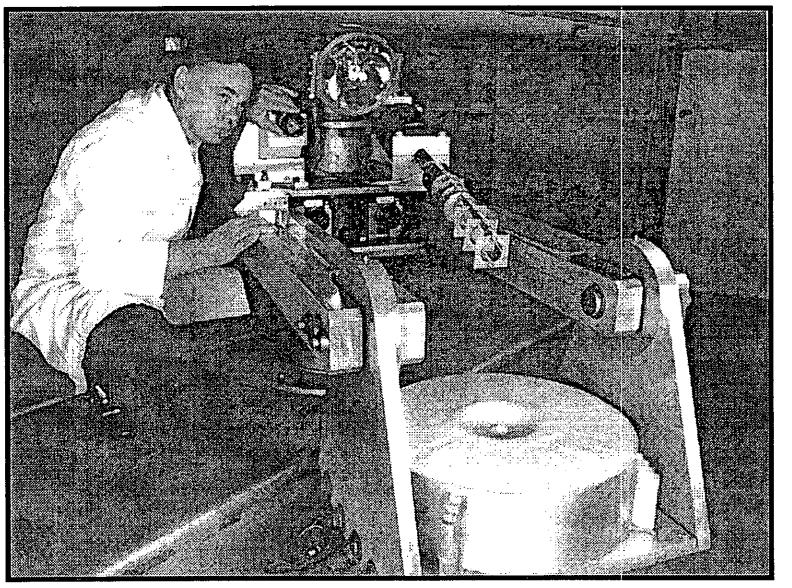

Figure 1. An impact crater formed in sand on the Boeing centrifuge. The technician is adjusting the lens of a high-speed film camera that sits just off the centrifuge spin axis. A gun is mounted on the other side. At the muzzle end of the gun are attached four blast shields and three break-wire screens for measuring projectile speed. The target sits in a basket that swings up 90° when the centrifuge spins.

A follow-up study was then conducted to examine how variations in crater size (i.e. variations in the centrifuge acceleration) and variations in bulk porosity affect the impact process. A total of twenty-four experiments were conducted at accelerations ranging from 1G to 500G and porosities ranging from 34% to 96%. Various results from this work were presented at two LPSCs and the Asteroids 2001 conference.

One of the main objectives of the experiments was to measure the total mass of material ejected beyond the crater rim. To facilitate this, a thin cloth was placed over the target surface with a hole centered on the impact point. The hole was made large enough such that the edge of the cloth was a few centimeters from the edge of the crater. In this way, essentially all ejecta could be collected on the cloth. Any material that fell in the

annular region between the crater edge and the inside edge of the cloth was easily collected by gently sweeping the thin crust that formed on the target surface during fabrication.

Figure 2 shows the post-impact target surface for six experiments. The three craters on the left side of the figure were formed at various accelerations in targets whose bulk porosity was 44%. The three images on the right side of the figure show corresponding results for targets with 70% porosity. In both cases, it is clear that the mass of ejecta decreases as the acceleration, i.e. simulated crater size, increases. In other words, small craters on a porous asteroid, such as those shown at 10G, eject a larger fraction of the crater mass than do large craters. It is also clear from Figure 2 that the craters formed in the material with 70% porosity have less ejecta than do those in the 44% target. In particular, the 500G crater in the material with 70% porosity ejected only a small amount of material, which is consistent with the experiments of Housen *et al.* (1999) discussed above.

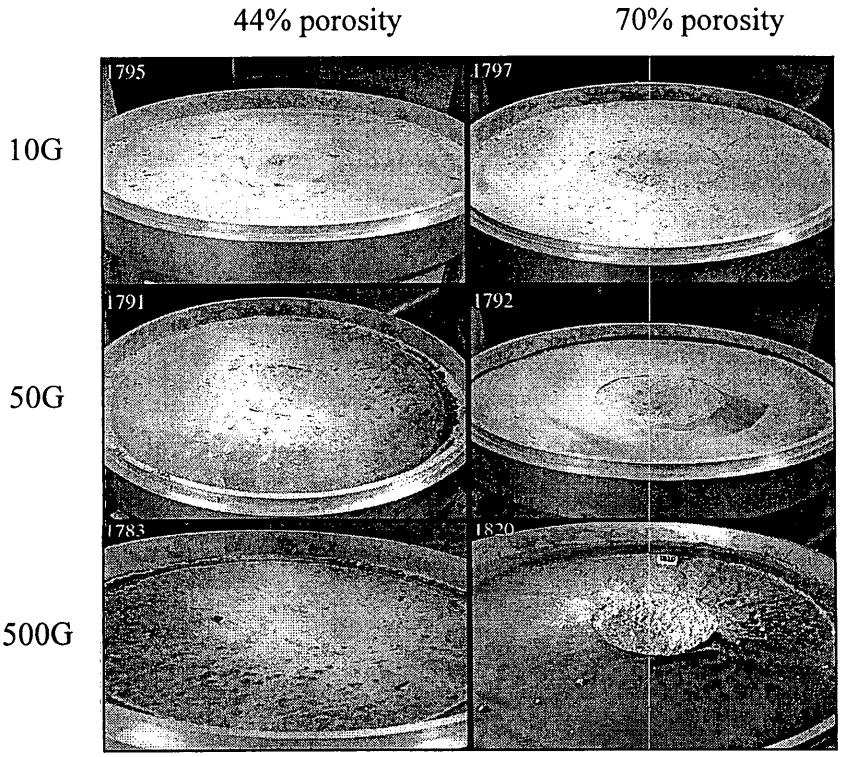

Figure 2. Results of centrifuge experiments in targets with porosity of 44% (left side) and 70% (right side). The black cloth was used to collect material ejected from the craters.

Figure 3 quantifies this behavior. The vertical axis shows the ratio of the mass of ejecta to the "crater mass", i.e. the mass of material originally contained within the crater bowl. Each of the curves shown in the figure, and the corresponding data through which the curves pass, represents a constant value of gD, where g is the acceleration and D is

the crater diameter, in cgs units. The value of gD is the scaled crater size for the experiment. Each curve shows that as target porosity increases, the amount of material in the ejecta blanket becomes a smaller fraction of the crater mass. At a fixed value of porosity, the mass ratio of ejecta also decreases as crater size (or gD) increases.

Figure 3 provides a way to directly apply the experimental results to kilometer-scale craters on asteroids. Each experimental point represents a direct simulation of an asteroid crater that has the same value of gD as the experiment. For example, crater Karoo on Mathilde has a value of $gD = 3.3 \times 10^6$ in cgs units ($g \sim 1$ cm/s^2, $D \sim 3.3 \times 10^6$ cm). Using a nominal porosity of 50%, the curves in the figure indicate that a Karoo-size crater would eject only about 10% of the crater mass beyond the crater rim.

Collectively, the results from the previous studies suggest that porous objects like Mathilde efficiently absorb the blow of large impacts, each of which compacts the asteroid and ejects very little material. Consequently, the original density of Mathilde could have been significantly lower than the presently observed value. These results are described in more detail in a paper just submitted to *Icarus* (Housen and Holsapple 2002), a preprint of which is attached to this report.

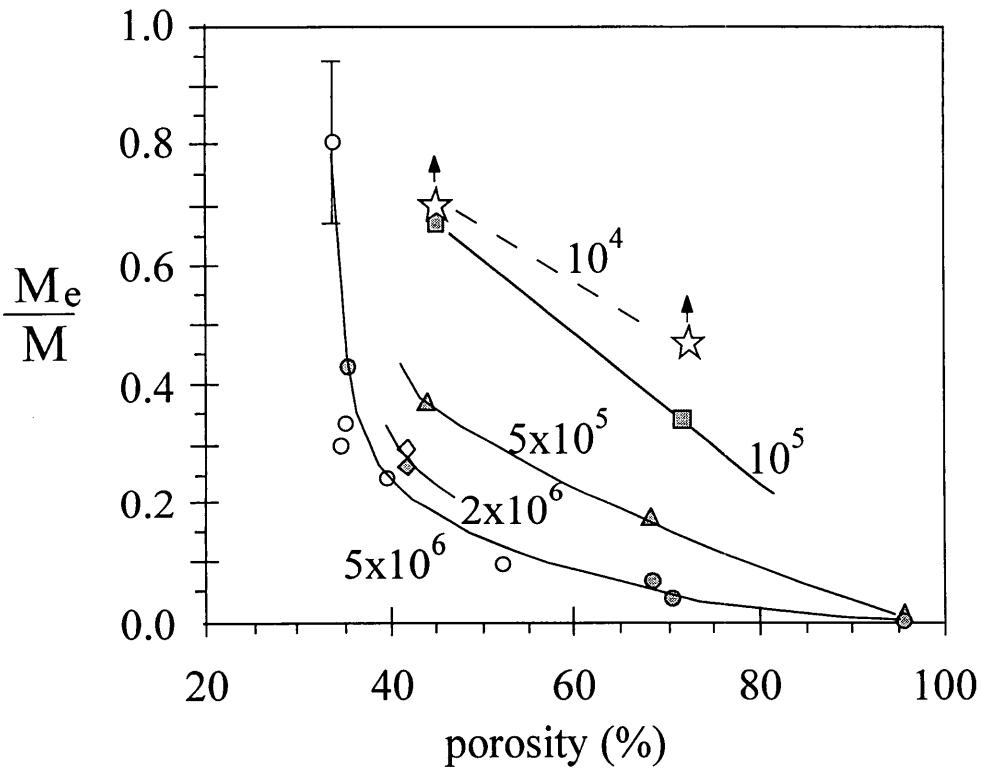

Figure 3. For a given crater size, the normalized mass of ejecta decreases as target porosity increases. Increasing porosity may cause a reduction in ejection velocity, so relatively more ejecta land inside the crater. Curves are labeled by their value of gD (cgs units).

Strength-Gravity Transition

The relative importance of target strength and gravity in determining crater size has been debated for many years. In the early studies of explosion cratering, gravity was though to play a negligible role, except for craters of very large size. In contrast, some of the early studies of impact cratering by D.E. Gault and R.M. Schmidt helped to define the conditions under which either strength or gravity are be the dominant factor in controlling crater size. The ratio $Y/\rho gh$ was shown to define the transition between the cases where strength or gravity dominates (Y=target strength, ρ=target density, g=gravity, h=crater depth).

Nolan *et al.* (1996) reported on numerical simulations of cratering that included a strain-rate dependent shock-damage model for rock. They noted that the shock front runs ahead of the transient crater bowl and pre-fractures the target material ahead of the cratering flow. Hence, most of the crater growth occurs in fractured material, which they assumed to be strengthless. Nolan *et al.* referred to this as a fracture-dominated regime because crater size is determined by the rate-dependent fracture strength of the material.

The assumption that fractured material is strengthless is incorrect. The relevant measure of strength in cratering in rock or moderately porous soils is the resistance to shear. Geological materials derive their shear strength both from cohesion and from the pressure-dependent resistance provided by internal frictional forces. This is often modeled by the Mohr-Coulomb relation: $Y = c + P\tan(\phi)$, where c is the cohesion, P is the confining pressure and ϕ is the angle of internal friction.

The pre-fracturing mechanism noted by Nolan *et al.* can reduce the cohesion to zero, but substantial shear strength can remain due to the frictional component. This effect can be seen in centrifuge experiments that we performed using targets comprised of layers of glass plates, as shown in Figure 4. A pre-impact view of the target is shown in the lower left corner of the figure. An impact at 500G extensively fractured the target and produced a small crater, as shown in the image in the upper right corner of the figure. A second impact into this pre-fractured material produced a crater of approximately the same size as the first impact. Even though the cohesion of the material had been reduced to zero, it still had substantial resistance to shear, owing to the frictional interlocking of the fractured target. Internal friction is an important mechanism that needs to be included in numerical simulations. Neglect of this mechanism undoubtedly contributes significantly to the fact that some code calculations have produced cratering efficiencies that are orders of magnitude larger than one would predict based on a substantial collection of explosion cratering data (Holsapple *et al* 2002).

The fracture-dominated regime is entirely consistent with the earlier ideas of a strength/gravity transition determined by the condition that $Y/\rho gh \sim 1$, as long as one uses the strain-rate dependent strength for Y. The work by Nolan *et al.* has emphasized the importance of determining the appropriate measure of strength that one uses for Y and the degree to which Y is dependent on loading duration or explicitly on the physical size of the event. For example, the fracture strength of rock is known to depend strongly on strain rate. But what about soils with moderate (~35%) or high (>50%) porosity?

Geological materials that are rate dependent are effectively weaker at large size scales because large events involve lower strain rates than do small events. Therefore, a

way to test for rate effects is to perform cratering experiments over a large range in size scale. As a result of this weakening, the cratering efficiency (cratered mass divided by the mass of the impactor) in rate-dependent materials increases with increasing event size.

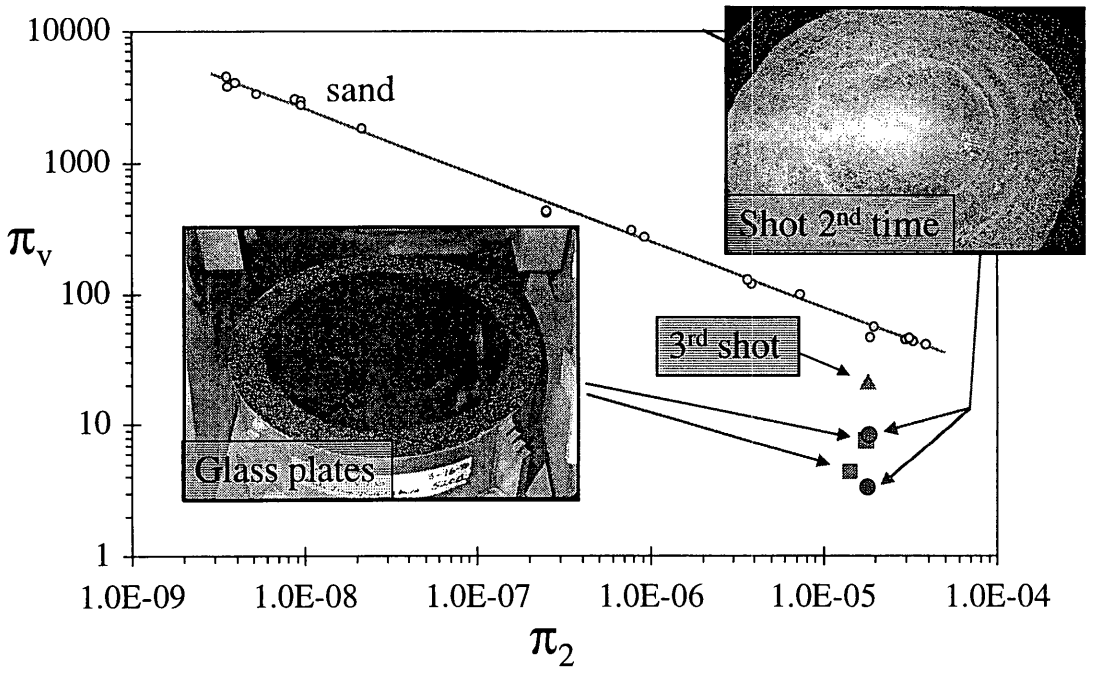

Figure 4. Centrifuge impact experiments using glass-plate targets. The first shot into this target extensively fractured the material and produced a small crater. A second shot into this pre-fractured material produced essentially the same crater size, showing the importance of the frictional component of shear strength in crater formation.

Laboratory cratering experiments generally do not involve a large enough variation in size scale to show this effect. However, field cratering tests using high explosives have been conducted with explosive mass varying over several decades. Figure 5 shows field data for three soils, dry sand, dry alluvium and playa, plotted in the form of cratering efficiency versus explosive mass. The results for cohesionless sand show a decrease in cratering efficiency with increasing explosive mass, as expected for gravity-dominated events. The data for playa exhibit an increase in cratering efficiency, which is indicative of a rate-dependent strength. In contrast, the dry alluvial soil exhibits no variation of cratering efficiency with event size.

Supporting laboratory data is provided by Schimming *et al.* (1965), who used a direct shear device to measure the quasi-static and dynamic shear strength of a variety of soils. Shear strength was found to be rate dependent only in soils containing more than about 15-20% moisture. The strength of dryer cohesive soils was found to be

independent of loading rate. Interestingly, the explosion cratering tests shown in Figure 5 for playa had significant moisture content (15-25%) whereas the alluvium explosion tests were performed in a much drier medium (4-12% moisture content). Therefore, the explosion results are consistent with the dynamic shear strength measurements. Both indicate that the shear strength of dry cohesive soils is not strongly dependent on strain rate.

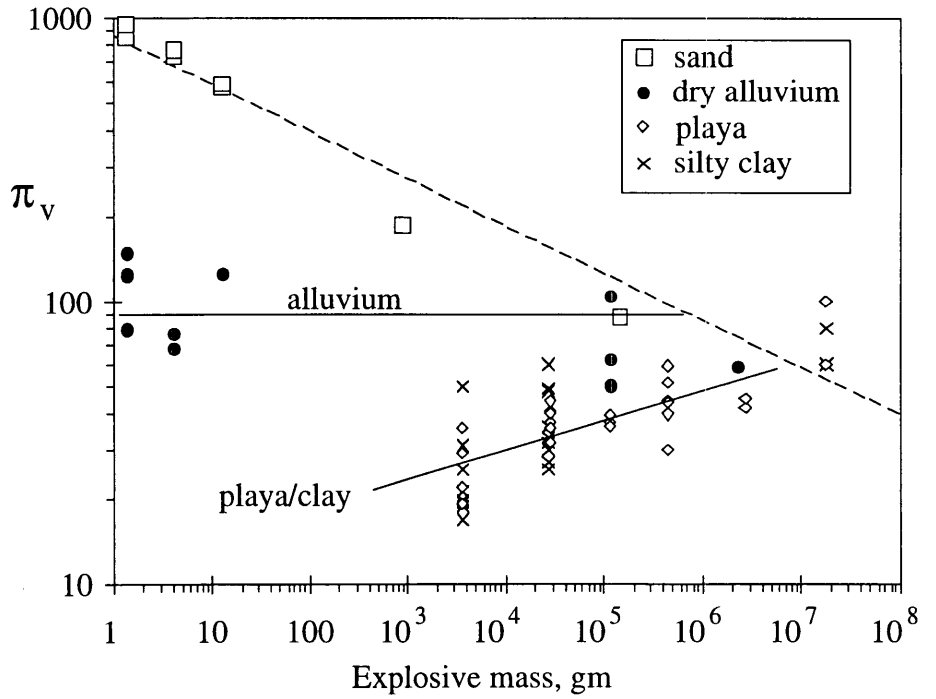

Figure 5. Results of explosive field cratering tests conducted in sand, playa and dry alluvium. All of the craters were generated by spherical high-explosive charges half-buried so that their center was coincident with the target surface. The increase in cratering efficiency of playa with increasing explosive mass is indicative of a strain-rate dependent strength. As discussed in the text, this is thought to be due to the high moisture content of the playa medium. The alluvium, which was quite dry, shows a constant cratering efficiency, which suggests the strength of this material is independent of strain rate.

Because moderately porous soils do not show a strong rate-dependent strength, the strength-gravity transition can be estimated from measurements of their static shear strength. Figure 6 shows the standard cratering efficiency plot for our results of impacts into porous materials. The data show a strength-dominated behavior (constant cratering efficiency), with a transition to gravity-dominance at about the value of π_2 expected based on the measured static strength.

The observed strength-gravity transition can be used to estimate the transition crater sizes for impacts on porous asteroids. The transition crater diameter D, normalized by the asteroid diameter is shown in Figure 7. The solid line indicates the midpoint of the undoubtedly broad transition region. Assuming that porous asteroids have about the same strength as the weak material used in the centrifuge tests, these results indicate that only bodies larger than about 30 km in diameter could have any gravity-dominated

craters. Crater Stickney would fall in the transition region between the two regimes. Mathilde's largest craters are big enough that they were undoubtedly affected by gravity

The transition region drawn in Figure 7 assumes that it is the shear strength that is the important strength measure for impacts on porous bodies. Although a strong argument can be made for this assumption for materials with moderate porosities of, say 30% to 40%, the situation for highly porous materials is less certain. As noted above, our experiments indicate that craters in porous targets form differently than those in typical soils. In porous materials, craters probably form mostly by permanent compaction of pore space, as opposed to the shearing and excavation processes that operate in less-porous soils. Therefore, it may be that a measure of the compaction strength is more important for highly porous soils. The implications of this possibility are still being studied and will be the subject of future experiments under this program.

The results of the strength-gravity transition study were presented at the 33rd LPSC. The slides from that presentation are attached as an addendum to this report.

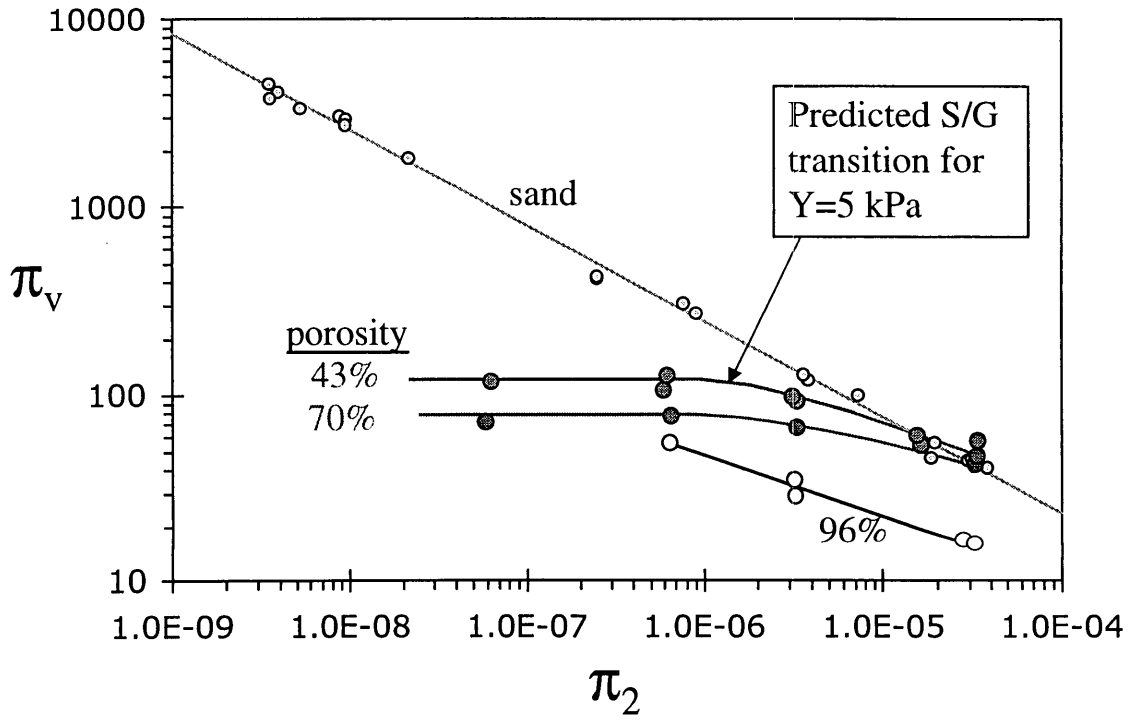

Figure 6. Cratering efficiency for impacts in porous materials. The materials with 44% and 77% porosity both show a constant cratering efficiency with a transition to a gravity-dominated regime at large values of π_2. The transition to the gravity regime is consistent with the strength measurements for these materials, as discussed in the text. Cratering efficiency is observed to decrease as target porosity increases.

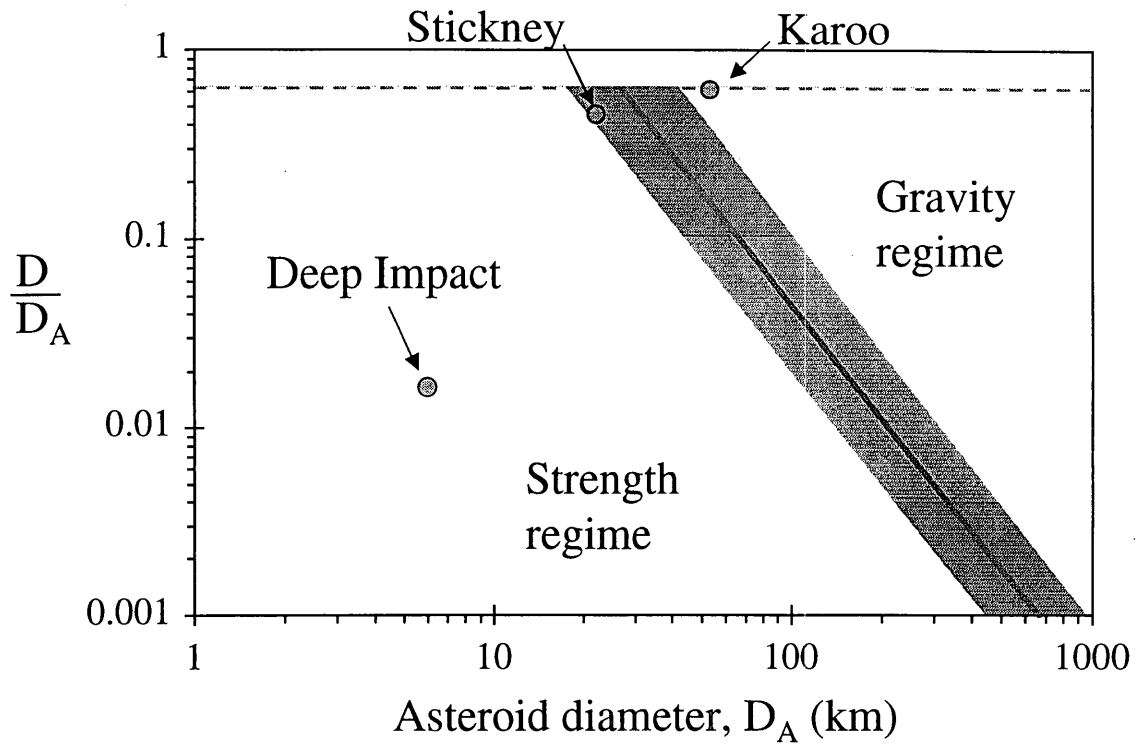

Figure 7. The crater diameter at which the strength-gravity transition occurs for impacts on porous bodies based on the results of centrifuge experiments. D is the crater diameter at the transition and D_A is the diameter of the body. If porous asteroids have about the same strength as the weak material studied here, then only bodies larger than about 30 km diameter would have any gravity-dominated craters.

References

ASPHAUG, E., OSTRO, S.J., HUDSON, R.S., SCHEERES, D.J. AND W. BENZ 1998. Disruption of kilometer-sized asteroids by energetic collisions. *Nature*, 393, 437-440.

BENZ, W. AND ASPHAUG, E. 1999. Catastrophic disruptions revisited, *ICARUS* **142**, 5-20.

Britt, D.T., Yeomans, D. Housen, K. and G. Consolmagno 2002. Asteroid porosity and structure. Submitted to ICARUS.

BRITT, D.T. AND G.J. CONSOLMAGNO S.J. 2000. The porosity of dark meteorites and the structure of low-albedo asteroids. *ICARUS*, **146**, 213-219.

CONSOLMAGNO, G.J. AND D.T. BRITT 1998. The density and porosity of meteorites from the Vatican collection. *Meteoritics Planet. Sci.*, **33**, 1231-1240.

FLYNN, G.J., MOORE, L.B. AND W. KLÖCK 1999. Density and porosity of stone meteorites: Implications for the density, porosity, cratering, and collisional disruption of asteroids. *ICARUS*, **142**, 97-105.

GREENBERG, J.M. 1986. Fluffy comets. *Asteroids, comets, meteors II; Proc. Int. Meeting*, Uppsala, Sweden, June 3-6, 1985, 221-223.

HOLSAPPLE, K.A. 1980. The equivalent depth of burst for impact cratering. *Lunar and Planet Science XI.*

HOLSAPPLE, K.A. AND R.M. SCHMIDT 1987. Point-source solutions and coupling parameters in cratering mechanics. *J. Geophys. Res.* 92, 6350-6376.

HOLSAPPLE, K.A., GIBLIN, I., HOUSEN, K., NAKAMURA, A. AND E. RYAN 2002. Asteroid impacts: Laboratory experiments and scaling laws. Submitted to *ICARUS.*

HOUSEN, K.R., SCHMIDT, R.M. AND K.A. HOLSAPPLE 1983. Crater ejecta scaling laws: Fundamental forms based on dimensional analysis. *J. Geophys. Res.*, **88**, 2485-2499.

HOUSEN K. R. AND HOLSAPPLE K. A. 1990. On the fragmentation of asteroids and planetary satellites. *Icarus 84*, 226-253.

HOUSEN, K.R., SCHMIDT, R.M. AND K.A. HOLSAPPLE 1991. Laboratory Simulations of Large Scale Fragmentation Events, *Icarus* **94**, 180-190.

HOUSEN, K.R , HOLSAPPLE K.A. AND M.E. VOSS 1999. Compaction as the origin of te unusual craters on the asteroid Mathilde, *Nature*, 402, 155-157.

HOUSEN, K.R AND K.A. HOLSAPPLE 2002. Impact cratering on porous asteroids. Submitted to *ICARUS.*

LOVE S.G., HORZ F. AND D.E. BROWNLEE 1993. Target porosity effects in impact cratering and collisional disruption. *ICARUS*, **105**, 216-224.

NOLAN, M.C., ASPHAUG, E., MELOSH, H.J. AND R. GREENBERG 1996. Impact craters on asteroids: Does gravity or strength control their size?. *ICARUS* 124, 359-371.

O'KEEFE, J.D., STEWART, S.T. AND T.J. AHRENS 2000. Impacts on comets and asteroids, *32nd Div. Planet. Sciences Mtg*, American Astronomical Society, abstract #07.01.

SCHIMMING B.B., HAAS, H.J. AND H.C. SAXE 1965. A comparison of the dynamic and static shear strengths of cohesionless, cohesive and combined soils. Air Force Weapons Lab. Tech Rept. *AFWL TR-65-48.*

SCHMIDT R.M. 1978. Centrifuge simulation of the JOHNIE Boy 500 ton cratering event, *Proc. 9th Lunar Planet. Sci. Conf.*, Vol 3, 3877-3890.

SCHMIDT, R.M. AND HOLSAPPLE, K.A. 1980. On the scaling of crater dimensions 1. Explosive processes, *J. Geophys. Res.*, **85**, 7247-7256.

SCHMIDT, R.M. AND K.R. HOUSEN, 1987. Some recent advances in the scaling of impact and explosion craters, *Int. J. of Impact Engr.* **5**, 543-560.

SCHULTZ, P.H., ANDERSON, J.L.B. AND J.T. HEINECK 2002. Impact crater size and evolution: Expectations for deep impact. *Lunar Planet. Sci. Conf. XXXIII*, abstract #1875 (CD ROM).

SIRONO, S. AND J.M. GREENBERG 2000. Do cometesimal collisions lead to bound rubble piles or to aggregates held together by gravity? *ICARUS*, **145**, 230-238.

STEWART, S.T. AND T.J. AHRENS 1999. Porosity effects on impact processes in solar system materials. *Lunar Planet. Sci. XXX*, abstract # 2020 (CD ROM).

WILKISON, S.L., ROBINSON, M.S., THOMAS, P.C., VEVERKA, J., MCCOY, T.J., MURCHIE, S.L., PROCKTER, L. AND D. YEOMANS 2001. The porosity of Eros and the implications for its internal structure. *Lunar Planet. Sci. XXXII*, Abstract 1721 (CDROM).

WILSON, L.L., KEIL, K. AND S.J. LOVE 1999. The internal structures and densities of asteroids. *Meteoritics Planet. Sci.*, **34**, 479-483.

Preprint of

Impact cratering on porous asteroids

K.R. Housen and K. A. Holsapple

Submitted to *Icarus*, 5/2002

Impact Cratering on Porous Asteroids

Kevin R. Housen

Physical Sciences, MS 2T-50
The Boeing Co.
P.O. Box 3999
Seattle, Washington 98124
e-mail: kevin.r.housen@boeing.com

Keith A. Holsapple

Dept. of Aeronautics and Astronautics, 352400
University of Washington
Seattle, Washington 98195
e-mail: holsapple@aa.washington.edu

Submitted to *Icarus*

Date: 5/3/02
Revised:
Pages: 31 (manuscript)
Tables: 3
Figures: 15

Proposed Running Head: Impact Cratering on Porous Asteroids

Send editorial correspondence to:

Dr. Kevin Housen

MS 2T-50

The Boeing Co.

P.O. Box 3999

Seattle, WA 98124

Voice: 206-544-5415

FAX: 206-544-5438

e-mail: kevin.r.housen@boeing.com

ABSTRACT

Increasing evidence that many or even most asteroids are rubble-piles underscores the need to understand how porous structures respond to impact. Experiments are reported in which craters are formed in porous silicate materials by impacts at 2 km/s. The experiments are conducted under conditions of elevated acceleration on a geotechnic centrifuge. In contrast to conventional small-scale experiments, centrifuge experiments provide conditions that reproduce the physics of the formation of asteroid craters as large as several tens of kilometers in diameter.

Crater and ejecta blanket formation in porous materials is found to be markedly different than observed in typical dry soils of low or moderate porosity. In porous materials, craters form mostly by compaction of the target material, and ejection velocities are lower than for impacts in less-porous materials. The experiments show that, while small craters on porous asteroids should produce ejecta blankets in the usual fashion, large craters form without ejecta blankets. In large impacts, most of the ejected material falls back into the crater. A significant crater bowl remains because of the volume created by permanent compaction of the target material. Over time, multiple cratering events can significantly increase the global density of an asteroid.

Key Words: Asteroids; Collisional physics; Cratering; Impact processes; Regoliths

I. INTRODUCTION

Although asteroids have long been suspected of having porous interiors (Chapman *et al.* 1977; Watson 1978), direct evidence of porosity has come only recently. Results from spacecraft missions and major improvements in ground-based optical and radar observation techniques have now provided reliable bulk density estimates for 22 asteroids (Britt *et al.* 2002). Ten of these objects have density less than 2.0 gm/cm^3, and 5 are below 1.5 gm/cm^3, which suggests that much of their interiors could be void space. Flynn (1994) noted that many interplanetary dust particles have high porosities, suggesting that the asteroids that they sample may be porous as well.

Quantitative estimates of porosity have been made by associating various taxonomic classes of asteroids with analogue classes of meteorites. The bulk porosity of an asteroid, i.e. the fraction of an asteroids volume that is void, is estimated from the known bulk density of the asteroid and the measured density of mineral grains in the corresponding analogue meteorite type. Such calculations show that many asteroids have significant pore space (Consolmagno and Britt 1998, Flynn *et al.* 1999, Wilson *et al.* 1999, Britt and Consolmagno 2000, Wilkison *et al.* 2001). For example, Britt *et al.* (2002) find porosities as high as 75%, with a clustering of objects in the range of 25-55%.

Comets are also thought to have highly porous structures. Empirical and theoretical data on the density of meteors, along with modeling of interstellar dust grain formation and aggregation indicate that cometary nuclei could have as much as 60-80% void space (e.g. Greenberg 1986, Sirono and Greenberg 2000).

Spacecraft observations of asteroid Mathilde strongly suggest that porosity has an important effect on the collisional evolution of asteroids. Mathilde, a C-type asteroid 66x48x46 km in size has a measured bulk density of ~1.3 gm/cm^3, and an estimated porosity of ~50% (Veverka *et al.* 1999, Britt *et al.* 2002). Aside from its low density, a surprising characteristic of Mathilde is that at least four giant craters are packed onto its surface, each

having a diameter that exceeds the mean radius of the asteroid[1]. Furthermore, even though these craters are closely packed, there is no evidence that the formation of one crater created any significant damage to its predecessors (Chapman and Merline 1999). In particular, there are no signs of seismic readjustments or ejecta deposition from these impacts.

Mathilde's high porosity is most likely responsible for the unusual appearance of its craters. Porous materials are known to efficiently absorb shock waves, which could allow craters to form in close proximity without jolting nearby craters. Additionally, the nature of impact ejecta on porous asteroids could be entirely different from that studied experimentally in the lab, where the target materials are usually of comparatively low porosity. Numerical simulations (Asphaug *et al.* 1998) indicate that impacts in porous targets eject material at high speeds, suggesting that most of Mathilde's ejecta would have escaped from the asteroid, leaving nearby craters undamaged. On the other hand, the experiments described in this paper indicate that large craters in porous materials form mostly by compaction and eject only a negligible amount of material beyond the crater rim. That is, Mathilde's craters do not exhibit substantial ejecta blankets because the craters did not eject very much material.

Studies by Kieffer (1975), Cintala *et al.* (1979), Asphaug *et al.* (1998), Davis and Ryan (1990), Nakamura *et al.* (1992), Stewart *et al.* (1999), O'Keefe *et al.* (2000), Schultz *et al.* (2002) and others have noted the effects of porosity on impacts (see Asphaug *et al.* 2002, Britt *et al.* 2002 and Holsapple *et al.* 2002 for extensive reviews). Even so, very little experimental work has focused on the problems of how porosity affects the mechanics of crater formation, crater scaling, and the formation of ejecta blankets. Love *et al.* (1993) reported on four impacts into porous targets made from sintered glass beads. Using thin foils as witness plates, they noted an absence of high-speed ejecta in the experiment involving the most porous (and weakest) target, suggesting that the ejecta speeds were lowest in the most porous target. Schultz *et al.* (2002) performed impact experiments in porous pumice targets and concluded that cratering efficiency (excavated mass divided by impactor mass) was about

---

[1] Only about half of Mathilde's surface was imaged, so there could well be even more of these large craters.

a factor of two smaller than that for dry sand, but exhibits the same gravity-dominated response with about the same power-law exponent as sand. That is not the conclusion here, which is discussed in more detail below.

A limitation of laboratory studies is that they are restricted to size scales of tens of centimeters, whereas large craters on asteroids occur at sizes of tens of kilometers. However, it is possible to bridge this gap in size scale by conducting impact experiments under conditions of high acceleration. Centrifuge experiments have been used to determine the scaling laws for impact cratering and to successfully simulate the formation of large terrestrial explosions craters (Schmidt 1978, 1980; Holsapple and Schmidt 1982; Schmidt *et al.* 1986).

Centrifuge experiments are useful because many important factors that affect crater size are proportional to the product of a linear crater dimension, (such as the depth h or radius R), times the gravitational acceleration g. For example, the shear strength of most geological materials is determined by the lithostatic stress ρgh, where ρ is the target density. The potential energy required to excavate a unit volume of material from the bottom of a crater is proportional to ρgh. The ballistic range of ejecta is a function of the product gR (Housen *et al.* 1983). Because these factors are all products of g and crater size, a large crater formed at low g is replicated by a small crater formed at high g. This fundamental basis for centrifuge modeling is discussed further in the next section.

Housen *et al.* (1999) conducted impact experiments in targets having a porosity of ~60%. Three experiments were conducted at 500G on a geotechnic centrifuge[2], which simulated the formation of craters the size of Mathilde's largest craters. The three experiments used a single target, with the impact points arranged in a triangular pattern such that the resulting crater rims were in close proximity to one another. Each impact was found to deposit only a very small mass of debris outside the crater rim. Additionally, the formation of the second and third craters produced no observable damage to the earlier craters unless the crater rims actually intersected. This is consistent with the suggestion that the pristine appearance of

Mathilde's large craters is the result of severe damping of the shock stress in porous materials. Furthermore, large craters in porous materials can apparently form without the ejecta blankets that have been a familiar signature of terrestrial and lunar impact craters.

Ejection of material during impact events is an important mechanism in the collisional evolution of asteroids. Excavation and deposition affect the exposure of meteoritic material to the solar wind and to cosmic rays, the degradation of extant craters and other surface features, and the distribution of blocks often observed on asteroid surfaces. The experiments reported here are designed as a first step in understanding how the excavation and deposition processes depend on target porosity and crater size. The next section describes the simulation method in more detail.

II. THE BASIS FOR CENTRIFUGE EXPERIMENTS

It may seem odd to use high-G experiments on a centrifuge to simulate impact events on asteroids such as Mathilde, whose gravity field is so weak that one could literally throw a rock faster than the escape speed. However, while gravity on such an asteroid is small, the largest craters are tens of kilometers in diameter. As a consequence, the lithostatic stresses at the bottom of these craters are about two orders of magnitude greater than those involved in craters formed at 1G in the lab. Therefore, correct simulation of large crater formation on asteroids requires that experiments be conducted at about two orders of magnitude elevated acceleration. We shall also show that 1G experiments can lead to incorrect conclusions regarding the ballistics of crater ejecta.

Formally, the use of a centrifuge in cratering studies is motivated through similarity analysis. This section defines the conditions for similarity, presents some scaling relationships that are used in the following sections, and discusses the strengths and weaknesses of centrifuge experiments.

---

[2] 1G is the acceleration of terrestrial gravity.

A. Conditions and implications of similarity

Suppose that a projectile of radius, a, density δ, and velocity U strikes a target under the influence of gravity g. The target material is represented by its density, ρ, a strength measure[3] Y, its porosity n, and a set, P_M of any further target or projectile material properties that have an effect on crater formation[4]. P_M can contain any parameters whose dimensional units can be constructed from stress and mass density scales, such as material strength or moduli. Velocity measures such as sound speed are also included because their units are obtained as a square root of stress divided by mass density. We exclude any size-dependent or rate-dependent properties, so P_M excludes any material properties that contain separate length or time scales. We also exclude any atmospheric pressure effects. The justification and consequences of these assumptions are discussed later.

A crater may be formed by excavation of material, by permanent compaction of pore spaces, or by structural uplift. Depending on the launch velocities, some of the excavated material may fall back into the crater, some may fall on the surface outside the crater, and some may exceed an asteroid's escape velocity and be lost. The symbols D and V are used to denote the diameter and volume of the crater after all material has landed (or escaped). The mass of material originally contained within the crater profile, i.e. the "crater mass", is denoted by M. The mass of material that falls back to the surface outside the crater, i.e. the "ejecta mass" is denoted by M_e.

The crater diameter is expressed as a function of the variables described above:

$$D = \mathrm{f}\,[a, U, \delta, \rho, Y, g, n, P_M]. \qquad (1)$$

---

[3] The question of *which* strength measure arises. As shown, similarity only holds between different events in the same material, so the question is moot. However, if one later wishes to look for scaling between different materials, with different strengths and different densities, then there is no obvious answer, since there always remains an arbitrary dependence on the material properties P_M. The assumption (hope?) is that there is a single dominant strength measure that determines the cratering, and that other material properties are not important. That is, it is assumed that the material is entirely characterized by one single strength measure, and a task of the analysis is to identify that measure. For normal dry soils, it is perhaps a shear strength, for porous materials it is perhaps a compressive strength.

[4] The porosity could be included in P_M, but because we will focus on its effects, it is explicitly noted.

The number of variables is reduced by three if they are expressed in non-dimensional form, i.e.

$$\frac{gD}{ga} = \mathrm{f}\left[\frac{ga}{U^2}, \frac{Y}{\delta U^2}, \frac{\rho}{\delta}, n, \pi_M\right] \qquad (2)$$

where π_M represents a set of non-dimensional ratios that involve only ρ, Y and the material properties contained in P_M.

Two impact events are *similar* when all of the non-dimensional ratios on the right side of Eq. (2) are the same for both events. One way to achieve this condition is to require that the following four quantities are the same for the two events:

1. target materials
2. impactor materials
3. impact velocity
4. the product ga

Under conditions 1 and 2, ρ/δ, n, and all of the ratios in π_M are the same because they involve only target and impactor material properties. With the addition of conditions 3 and 4, the remaining terms on the right side of Eq. (2) are also the same. Hence, a consequence of the conditions listed above is that the value of gD is the same for any two similar impacts.

Consider a projectile of radius a_A that impacts an asteroid and produces a crater of diameter D_A. In a corresponding centrifuge experiment, a projectile of radius a_C produces a crater of diameter D_C. The conditions of similarity guarantee that

$$a_A = (g_C/g_A)\, a_C. \qquad (3)$$

$$D_A = (g_C/g_A)\, D_C. \qquad (4)$$

Dividing Eq. (4) by Eq. (3) also shows that the ratio of crater diameter to impactor diameter, D/a, is the same for both events.

The above argument also applies to any other linear measure of crater size, such as the depth, rim height, and so on. As a result, the centrifuge crater is a geometric replica of the asteroid crater, which is a factor of g_C/g_A larger in all linear dimensions.

Centrifuge experiments are especially useful in simulating crater formation on asteroids, because of the large linear scale factor g_C/g_A. Using Mathilde as an example, where $g_A \sim 10^{-3}$G, a 500G centrifuge simulation provides a length scale factor of 5×10^5. Hence, the largest craters on Mathilde, with diameters of 20 to 30 km, are simulated by 500G centrifuge craters having diameters of several centimeters.

The conditions for similarity also hold for ejecta. The total ejecta mass can be written as a function of the same variables listed in Eq. (1) and expressed in non-dimensional form as

$$\frac{M_e}{\rho a^3} = \mathrm{f}\left[\frac{ga}{U^2}, \frac{Y}{\delta U^2}, \frac{\rho}{\delta}, n, \pi_M\right] \tag{5}$$

Under the conditions for similarity defined above, all of the terms on the right side of this equation are the same for two similar events, i.e.

$$\left[\frac{M_e}{\rho a^3}\right]_C = \left[\frac{M_e}{\rho a^3}\right]_A \tag{6}$$

where the subscripts A and C again refer to the asteroid and centrifuge craters respectively. As noted above, the ratio D/a is the same for similar events, so that Eq. (6) is equivalent to

$$\left[\frac{M_e}{\rho D^3}\right]_C = \left[\frac{M_e}{\rho D^3}\right]_A \tag{7}$$

Hence, the centrifuge experiment reproduces the ratio of the mass of ejecta to the crater mass that occurs in the asteroid impact.

A centrifuge is actually not required to simulate small cratering on asteroids. Again using Mathilde as an example, the length scale factor for a 1G experiment is 10^3. So, a 10 cm crater at 1G in the lab is equivalent to a 100m crater on Mathilde; but at 500G that same 10 cm crater is equivalent to a 50 km crater. The crater shape and ejecta mass ratio M of the

10cm crater formed at 1G may be quite different from the 10cm crater formed at 500G. This is the raison d'être for centrifuge experiments.

B. Scaling relationships

The conditions for similarity connect a given subscale laboratory experiment to a given larger crater on an asteroid. Scaling relationships relate the results between a set of *non-similar* experiments obtained, for example, by varying size, gravity, or velocity. These relationships are typically suggested by theoretical assumptions compared to a sequence of subscale experiments. For example, scaling relationships can be derived by noting that, to a very good approximation, the impactor is a point source (see Holsapple and Schmidt 1987 for details). In that case there cannot be independent measures of the impactor size or time. Therefore, the radius a (size scale), velocity U (a/U is a time scale) and density of the impactor δ, cannot be important separately, but only in some specific power-law combination $C = aU^{\mu}\delta^{\nu}$, where μ and ν are scaling constants, with ν typically equal[5] to 1/3. The exponent μ can range from 1/3 to 2/3; end member cases that correspond to momentum scaling and energy scaling (because in those cases C is proportional to the cube-root of the impactor momentum or energy respectively). Target porosity is known to have a strong effect on μ, with higher porosities tending more toward the momentum scaling limit. For dry sand, with a porosity of ~30% to 35%, μ has been measured to be ~0.4 (Schmidt, 1980; Holsapple and Schmidt, 1987), while for water μ~*0.6,* nearer the energy limit.

The point-source assumption reduces the number of parameters by two more, giving in various important cases definite power-law scaling relationships. Those for crater size have been derived by Holsapple and Schmidt (1987), and are summarized[6] here in Table 1 for reference. Corresponding relationships for mass ejected outside the crater can be derived by

---

[5] If the important impactor measures are its mass and velocity, and not its size, then $\nu = 1/3$

[6] Since we focus here on the effects of target porosity n, that dependence has been added to the previous forms.

expressing it in terms of the point-source measure C and the variables related to the target, i.e.

$$M_e = \mathrm{f}\,[C, \rho, Y, g, n, P_M]. \tag{8}$$

An analogous expression for the crater diameter is

$$D = \mathrm{f}\,[C, \rho, Y, g, n\,, P_M]. \tag{9}$$

Equation (9) can be used to eliminate C from Eq. (8), which gives

$$M_e = \mathrm{f}\,[D, \rho, Y, g, n\,, P_M] \tag{10}$$

In non-dimensional form, this becomes

$$\frac{M_e}{M} = \mathrm{f}\left[\frac{Y}{\rho g D},\ n,\ \pi_M\right]. \tag{11}$$

The usual practice in studies of cratering is to consider two limiting regimes, when one of material strength or gravity has the dominant effect on crater formation. For example, if we suppose that the lithostatic stress ($\rho g D$) is much larger than the strength of the target material, then the strength properties become unimportant and can be ignored in Eq. (11). Hence, in the gravity regime, the ejecta mass fraction M_e/M is independent of crater size and depends only on material type. This is consistent with the conclusion of Housen *et al.* (1983) that craters and ejecta blankets of all gravity-regime craters in a given material are geometric replicas of one another.

[Table I]

In the opposite limit, lithostatic stress is small compared to material strength, the role of gravity can be neglected, and the ejecta mass fraction in Eq. (11) again reduces to a constant (at least for fixed materials, so that all variables in π_M are constant). Physically this due to the fact that ejecta velocities in the strength regime (such as in a small crater formed in rock) are typically high enough that all ejecta are deposited far from the crater rim. In this case, variations in crater size do not affect the fraction of ejecta deposited outside the crater rim.

However, the constant value assumed by the mass fraction in the strength regime need not be the same as in the gravity regime

Additional comments regarding ejecta scaling are in order. First, the transition between the strength and gravity limit regimes could be quite broad, and the ejecta mass fraction may depend on crater size in this transition region. Second, while materials with no cohesion and moderate porosity (e.g. dry sand) clearly exhibit a gravity regime, the existence of a gravity regime for highly porous materials has not yet been definitively established. Porous materials may respond to impacts in an entirely different manner than do the materials that have been studied in the lab. The assumption of a point source coupling measure may not be valid; or gravity and strength may not be separable. For example, impacts into porous materials form craters mostly by permanent crushing and compaction of the target material, so it would be reasonable to assume that crater size and ejecta velocities depend on some measure of the crushing strength of the material. However, on large porous asteroids, lithostatic stresses could exceed the crushing strength of the material, in which case the asteroid would self-compact until reaching a state where the local lithostatic stress is comparable to the crushing strength of the compacted material. Large craters formed in such materials may never reach a truly gravity dominated regime because, by definition, gravitational stresses would always be of the same order as the crushing strength.

C. Uncertainties in the present centrifuge tests.

Centrifuge testing currently provides the only experimental method for studying large-scale cratering on asteroids. A major benefit is that one can effectively vary crater size over three orders of magnitude by varying the centrifugal acceleration. However, as with any method (including numerical simulation), centrifuge experiments cannot provide an exact simulation of large impacts on asteroids.

The present experiments use targets with flat surfaces, while large impacts on asteroids may be affected by local surface curvature[7]. As described by Fujiwara *et al.* (1993), craters formed on a curved surface tend to be larger than those produced by the same impactor on an expansive flat surface. Increasing the surface curvature causes the crater diameter to increase slowly by about 15%. When the radius of curvature is comparable to the radius of the flat-surface crater, the crater increases sharply in size and becomes convex in shape rather than convex. The abrupt increase in size appears to result from spallation of the mortar targets used by Fujiwara *et al.;* whether that same result holds for other materials is unknown. Considering the efficiency with which porous materials damp shock stress, the effect of surface curvature may also be reduced on porous asteroids. This question should be addressed in future experiments.

We assume that none of the material properties in P_M contain any separate length or time scales, i.e. we assume that the target materials are not rate-dependent or size-dependent. This assumption is certainly *not* valid for impact disruption of brittle materials, like rock, whose strength is known to decrease substantially with either increasing size scale or loading duration (Housen and Holsapple 1999). However, the present study considers cratering in dry porous soils, for which there is evidence to support the assumption that strength is not strongly dependent on strain rate or size scale, as now described.

Geological materials that are rate dependent are effectively weaker at large size scales because large events involve lower strain rates than do small events. Therefore, a way to test for rate effects is to perform cratering experiments over a large range in size scale. As a result of this weakening, the cratering efficiency (cratered mass divided by the mass of the impactor) in rate-dependent materials increases with increasing event size.

Laboratory cratering experiments generally do not involve a large enough variation in size scale to show this effect. However, field cratering tests using high explosives have been

---

[7] Samples with a curved surface could be tested; but, of course, the central force field of self-gravity could not be simulated.

conducted with explosive mass varying over several decades. Figure 1 shows field data for three soils, dry sand, dry alluvium and playa, plotted in the form of cratering efficiency versus explosive mass. The results for cohesionless sand show a decrease in cratering efficiency with increasing explosive mass, as expected for gravity-dominated events (Table I). The data for playa exhibit an increase in cratering efficiency, which is indicative of a rate-dependent strength. In contrast, the dry alluvial soil exhibits no variation of cratering efficiency with event size.

[Figure 1]

Supporting laboratory data is provided by Schimming *et al.* (1965), who used a direct shear device to measure the quasi-static and dynamic shear strength of a variety of soils. Shear strength was found to be rate dependent only in soils containing more than about 15-20% moisture. The strength of dryer cohesive soils was found to be independent of loading rate. Interestingly, the explosion cratering tests shown in Figure 1 for playa had significant moisture content (15-25%) whereas the alluvium explosion tests were performed in a much drier medium (4-12% moisture content). Therefore, the explosion results are consistent with the dynamic shear strength measurements. Both indicate that the shear strength of dry cohesive soils is not strongly dependent on strain rate.

Simulations of terrestrial explosion craters, for which both the initial conditions and final crater size are known, have provided compelling evidence for the validity of the centrifuge method. Figure 2 shows an example. The centrifuge test used the same alluvial soil as the field test and an acceleration that satisfied the conditions for similarity. As shown in the figure, the small-scale centrifuge simulation agreed very well with the 20 ton explosive field test. Other large field tests have also been simulated with good success but, for reasons of brevity, are not shown here.

[Figure 2]

III. EXPERIMENTS

The Boeing geotechnic centrifuge was used to conduct the high-G tests. This facility has a maximum rated acceleration capability of 600G. A powder gun is mounted on one of the centrifuge arms near the spin axis. Blast shields are mounted at the muzzle of the gun. Three break-wire screens are mounted outboard from the blast shields and are used to obtain two measurements of projectile velocity. All of the tests used cylindrical high-density polyethylene projectiles of diameter 12.2 mm, density 0.93 gm/cm^3, and a nominal velocity of 1.9 km/s.

Porous targets were made from a mixture of F75 quartz sand, perlite, fly ash and water. Perlite is a naturally occurring siliceous volcanic rock. In its crude form, perlite contains a few percent of combined water. Expanded perlite, like that used here, is manufactured by rapidly heating the crude rock to at least 870°C at which point the combined water vaporizes, causing a sudden and significant increase in volume, and porosity. The result is a white, highly porous, easily crushable material. The perlite used here had a bulk density of 0.12 gm/cm^3. The particle size distribution, determined from a sieve analysis, is shown in Fig. 3. Fly ash is a cementing agent that was used to prevent the sand and perlite from sorting during the mixing and curing process.

[Figure 3]

By adjusting the relative proportions of the components, targets were made with porosity ranging from about 34% (pure sand) to about 96% (pure perlite). Most of the targets were made using four mixtures, summarized in Table II. The table also shows the grain density, ρ_g, of each component and the typical bulk density if a single component is poured into a container. After the materials for a given target were combined, the mixture was scooped into a steel bowl, 40.6 cm in diameter. The surface was leveled with a screed. The target was allowed to cure overnight, and then placed in an oven at approximately 90C for three days. Samples were removed and weighed periodically to assure removal of all water. Table II shows the typical bulk density and porosity of the material after drying. Note that the actual

porosities obtained for each target differ slightly from that shown in Table II due to unavoidable variations in how the material was emplaced in the container. The porosity for each test was determined from the measured bulk density of the target and the grain densities shown in Table II.

[Table II]

Standard cylindrical samples (5.0 cm diameter, 10.2 cm high) were also poured for static strength tests. Figure 4 shows that all of the materials were quite weak. Except for the least porous materials, the uniaxial compressive and tensile strengths were typically $2x10^5$ dynes/cm^2 and $4x10^4$ dynes/cm^2 respectively. For comparison, the static compressive strength of weak soils is typically in the range of $3x10^5$-10^6 dynes/cm^2 (Lambe and Whitman, 1969).

[Figure 4]

The two limit cases of pure perlite and pure sand did not use any water or fly ash. The pure sand targets were prepared by slowly raining dry sand through a sieve into the target container. This provided a bulk density of 1.75 gm/cm^3, which is very close to the maximum possible density ("fully dense") state. For the 100% perlite targets, the perlite was simply poured carefully into the container to minimize size sorting of the particles.

The target container was placed in a cylindrical fixture 46 cm in diameter on the centrifuge. The volume between the container and the cylindrical fixture was filled with sand to keep the sample in place and to provide an approximate match to the mechanical impedance of the target material.

In some experiments, a thin silk cloth was used to facilitate collection of ejecta. The cloth covered the surface of the target and included a circular hole whose diameter was larger than that of the expected crater and whose center was at the impact point. Typically, an initial test was performed without the cloth to determine the diameter of the hole needed to accommodate the crater The cloth generally did not extend closer than a few cm from the crater edge. Comparisons of crater profiles from experiments with and without the cloth

showed that the cloth had no effect on crater size. After a test, the cloth was carefully removed so that the mass of ejecta on it could be determined. The material collected on the cloth is a lower bound on the total ejecta mass because some material could fall in the annular region outside the crater rim but inside the inner edge of the cloth. Fortunately, the targets containing fly ash typically had a mm-thick weak crust on the surface which permitted collection of ejecta by gently sweeping with a fine brush. This allowed collection of any remaining ejecta in the annular region. The crust also allowed ejecta to be collected in cases where the cloth was not used, e.g. in the initial tests performed to determine the hole size for the cloth.

While these methods allowed collection of material that fell on to the target surface, any material that landed off the centrifuge fixture was lost. To guarantee collection of all ejecta, some experiments employed a lid over the target fixture. A hole was cut into the top of the lid to allow passage of the projectile.

Several pairs of tests were conducted to assess any effects that the lid had on crater formation. Figure 5 shows representative results of three such pairs of tests. The crater profiles from the tests that used the lid are shown with heavy lines. At high G (tests 1785 and 1786, 508G), and at 50G the lid had no discernable effect on the crater or ejecta profile. At 10G the lid does have a noticeable (though small) effect; because the ballistic range of ejecta is large enough in this case that some material may strike the lid and bounce back into the crater bowl.

[Figure 5]

The lid was also used in one test to determine the effects of atmospheric drag on the ejecta. In that test (shot 1820), the projectile entrance hole was covered with aluminum foil, taped at the edges. The lid was placed over the target and helium gas was slowly bled into the volume above the target surface, replacing the existing air. After a period sufficient to fill the volume several times over, the gas was turned off. A leak checker was used to assure that no significant leakage of helium occurred over a time period comparable to that required for

completion of a centrifuge test (typically a few minutes). This provided an atmosphere with a pressure of 1 bar, but a density that was a factor of 7.2 lower than in the other experiments. Any significant effects of atmospheric drag should then be reflected in the ejecta blanket, and perhaps the crater. As discussed in the next section, the helium atmosphere had no measurable effect on either the ejecta mass or crater volume. Therefore, it is reasonable to ignore atmospheric effects in the present experiments. This is, discussed below in more detail.

Crater profiles were measured using a profilometer with probes spaced 6 mm apart. Profiles were measured along two diameters and were used to determine crater depth, diameter and volume. Note that the crater diameters reported here are apparent (not rim) values, i.e. they represent the distance between the diametrically opposed points where the crater profile intersects the target surface.

The experimental results are summarized in Table III, which is sorted into groups of constant target material composition. In the column labeled C/L, the letters C and L indicate whether or not the ejecta collector cloth or the lid were used in a given experiment. In some cases, the mass of ejecta could not be measured and the corresponding entry in the table is blank. This was the case for the pure sand experiments (shots 1785 and 1786), and for the pure perlite tests that did not employ the collector cloth. In the cases where the collector cloth was not used, but an ejecta mass is shown in the table, the target surface had a thin crust that allowed ejecta to be collected by sweeping, as discussed above.

[Table III]

IV. CRATER SHAPE AND SIZE

Figure 6 shows how the crater profile varies with acceleration, for three values of the target porosity. The top part of Figure 6 shows the results for a moderately porous (44%) target. The crater size decreases with increasing g, but the crater shape does not vary markedly. The targets with 70% porosity show a much different behavior. As g increases,

the crater radius is relatively constant, but the depth decreases dramatically. As discussed in the next section, the mass of ejecta also decreases as g increases. Hence, the reduction in crater depth at high accelerations may be due to the fact that relatively more material falls back into the crater. The targets made from pure perlite showed yet a third behavior: the crater radius decreased sharply with increasing g, while the depth was nearly constant. This may be due to the fact that, while the perlite had very little cohesion initially, the self-compression at high g compressed the material and resulted in a noticeable increase in cohesion. As evidence, after the 500G test (shot 1808), large chunks of the target material could be handled (gently) without breakage. The compression of the material is evident in the profile for shot 1808. The elevation increases with increasing distance outwards from the crater edge because the target was deeper in the center than at the edge and therefore compressed more in the central regions. The larger cohesive strength of the material at high g may have been responsible for the smaller crater radius.

[Figure 6]

Figure 7 illustrates the effect of target porosity at fixed g. At high g (i.e. large crater size on an asteroid), the craters increase in size as porosity increases, with a dramatic increase as the porosity increases beyond 70%. Similar behaviors are exhibited by the results at 50G and 10G.

[Figure 7]

It is important to understand the mechanisms that govern the formation of craters, not only to attain a fundamental understanding of the cratering process, but also because the extrapolation of laboratory experiments to asteroid impacts depends very much on these mechanisms. To what degree is crater size in porous materials determined by material strength, porosity, or gravity?

The relative importance of target strength and gravity can be examined by plotting crater size measurements in the non-dimensional form given in Table I. For example, if gravity is the single factor determining crater size, the cratering efficiency is given by

$$\frac{\rho V}{m} = f_{Vg}(n)\,(\rho/\delta)^{(2+\mu-6\nu)/(2+\mu)}\,\pi_2^{-3\mu/(2+\mu)} \qquad (12)$$

whereas if a single strength[8] is the predominant factor,

$$\frac{\rho V}{m} = f_{Vs}(n)\,(\rho/\delta)^{1+3\mu/2-3\nu}\left(\frac{Y}{\delta U^2}\right)^{-3\mu/2}. \qquad (13)$$

Therefore, in the standard plot of $\log(\rho V/m)$ versus $\log(\pi_2)$, the strength regime is represented by horizontal lines whose vertical position decreases as a power of $Y/\delta U^2$ and may also depend on the density ratio ρ/δ and the target porosity. The gravity regime is represented by a straight line whose slope is $-3\,\mu/(\mu+2)$, and again with a possible dependence on density ratio and target porosity. The density dependences are considered below.

Figure 8 shows the cratering efficiency for the porous targets, along with data for Ottawa Flintshot sand (Schmidt 1980). The craters formed in cohesionless sand are completely gravity dominated and show the expected straight line on the log-log plot. The slope of the line is -0.51, which gives μ=0.41. The results for the targets with 44% and 70% porosity clearly show evidence of strength-dominated behavior for small values of π_2, with an incomplete trend toward gravity dominance at the largest values of π_2. Note, while the 70% porous craters are larger in volume than the 44% craters, they are smaller in crater mass.

[Figure 8]

We now investigate the assumption that the compressive strength and mass density determine the differences in cratering between the 44% and 70% targets, separately from the porosity. The cratering efficiency for 70% porosity is about a factor of 1.7 smaller than that for the material with 44% porosity. This cannot be a result of differing compressive strengths for the two materials, because Figure 4 shows that they have about the same

[8] Again, this assumes there is in fact one single strength measure that, together with the mass density, suffices to characterize the target materials. Here we consider the assumption that the compressive strength assumes that

strength. Therefore, it is instructive to compare to the density dependences given in Eqs. (12) and (13) given above to see if that could be the defining criteria.

The effect of target density can be estimated for reasonable values of the scaling exponents μ and ν and using Eqs. (12) and (13). The value of μ is known to be 0.4 for dry sand as shown above. Materials with higher porosity are expected to have lower values of μ (Holsapple and Schmidt 1987), but no lower than the momentum-scaling limit of 1/3 (Holsapple and Schmidt 1982). A value of 1/3 is adopted for the density exponent, ν. Under these assumptions, Eqs (12) and (13) show that the cratering efficiency is proportional to the target density raised to a power of 0.14 to 0.17 in the gravity regime, and 0.50 to 0.60 in the strength regime. The ratio of densities for the materials with 44% and 70% porosity is about 2. This should produce about a factor of 1.4 to 1.5 change in the cratering efficiency, which is slightly smaller than the observed ratio of 1.65 (Table III). In the gravity regime, this same factor of 2 change in density should produce a factor of 1.1 variation in cratering efficiency, which is again smaller than the observed ratio of 1.25. While not conclusive, these results indicate that target porosity is partly responsible for the reduction in cratering efficiency observed for the targets with 70% porosity.

Additional insight can be gained by considering the results for the pure-perlite targets, which had a porosity of 96%. The cratering efficiency for this material is a factor of 3.2 lower than for the material with 44% porosity. The ratio of densities for these materials is 15, which should produce a factor of 1.5 change in the cratering efficiency in the gravity regime, using the assumptions noted above.

It would appear that the strength and density scaling in Eq. (13) does not suffice to describe the results, so target porosity itself becomes the likely candidate for describing the differences in the strength regime. More study is warranted.

---

role. However, another significant material property is simply the porosity, so the scaling between different materials need not be determined by any single strength.

V. EJECTA MEASUREMENTS

The experiments with the collector cloth showed how the mass of ejected material depends on target porosity and on event size (i.e. gD). Figure 9 shows the results of six experiments. The three images on the left side of the figure are from impacts into targets with 44% porosity at three accelerations. The three images on the right are for targets with 70% porosity. A visual comparison of these images clearly shows that the mass ratio of ejecta decreases as target porosity increases and as the simulated crater diameter increases. Notice in particular that the impact at 500G and 70% porosity ejected just a very small amount of material.

[Figure 9]

Figure 10 shows quantitatively how the ejecta mass fraction varies with the simulated crater diameter. For a given target porosity, the mass fraction steadily decreases as gD increases. The scale along the top horizontal axis in the figure shows the simulated crater diameter for an asteroid with g=1 cm-s^2, such as Mathilde. These results show that small impacts on a porous asteroid will eject a much larger fraction of the crater mass than large impacts.

[Figure 10]

Figure 11 shows the same results, but emphasizes the effect of target porosity. Each curve in the figure, which corresponds to a fixed value of gD, shows a decrease in the ejecta mass fraction as the target porosity increases. Experiments that used the lid are shown by filled symbols; those that did not are shown by open symbols. In most cases, the results from experiments that used the lid lie quite close to those that did not, indicating that the hollow symbols provide reasonable estimates of the ejecta mass fraction. The 1G experiments are an exception. In those experiments, the ballistic range of ejecta was expected to be large enough that the lid would interfere with ejecta trajectories, so the lid was not used. Consequently, some of the ejected material was undoubtedly lost. The 1G tests were conducted inside a horizontal cylindrical chamber roughly 1 m in diameter and 2 m long. The

chamber was swept clean before a test, and swept again after, thus allowing most of the material that landed off the target fixture to be collected. However, difficulties in accessing certain parts of the chamber prevented collecting all material. Hence, the ejecta mass from the 1G tests may be larger than that reported here.

[Figure 11]

The results shown in Figures 10 and 11 show that large craters in porous materials eject only a small fraction of the crater mass to locations beyond the crater rim. This is markedly different than typical impact experiments that use targets of low or moderate porosity. For example, impacts into sand always show substantial ejecta blankets. What mechanism is responsible for the lack of ejecta in highly porous targets?

All of the experiments were conducted under a pressure of one atmosphere. Perhaps aerodynamic drag on the ejecta particles was large enough to prevent ejecta from being deposited outside the crater rim. Experiments have shown that atmospheric pressure and aerodynamic drag affect crater formation under certain conditions (Johnson *et al.* 1969, Schultz and Gault 1979, Schultz 1982, Schmidt 1992, Schultz and Barnouin 1994). For example, the pressure of the overlying atmosphere reduces crater size when the pressure exceeds the lithostatic stress (Holsapple 1980, Schultz 1982). In addition, if ejecta particles are sufficiently small, aerodynamic drag reduces the ballistic range enough to affect crater size and the morphology of the ejecta blanket (Schultz 1992, Schmidt 1992; Schultz and Barnouin 1994; Barnouin-Jha and Schultz 1998). However, these effects are greatly reduced in high-G centrifuge tests, because the time interval that ejecta particles are subjected to drag forces is much smaller than in a test conducted at 1G.

Schmidt (1992) reported on centrifuge experiments using shallowly-buried explosive charges, which are known to be good analogues of impact (Holsapple, 1980). The experiments used various types of sand, atmospheric gasses and pressures. Figure 12 shows how cratering efficiency depends on atmospheric pressure for the centrifuge experiments and the 1G impacts reported by Schultz (1992). The 1G impact results for F-140 sand (median

grain size ~ 100 μ) and pumice (median grain size ~ 80 μ) show a stronger dependence on pressure than do the 22G and 488G centrifuge experiments. Even finer sands (20μ grain diameter), for which aerodynamic drag should be enhanced, indicate only a minor effect on crater size at high G. Therefore, the one-atmosphere of ambient pressure most likely had no significant effect on crater size in the centrifuge experiments.

[Figure 12]

Additional evidence indicates that aerodynamic drag had a negligible effect on crater size. Shot 1820, was conducted in a helium atmosphere (pressure=1 bar). Hence, the drag forces, which are proportional to the density of the atmosphere, were a factor of 7.2 less than in shot 1788, which used air as the atmosphere. The crater profiles for these two shots were indistinguishable, which indicates that atmospheric drag had no significant effect on crater size. Furthermore, if drag were important in these experiments, one would expect to see some sorting of the ejecta particles, with the low-density perlite fragments being deposited closer to the crater rim than the denser sand grains. No such sorting was observed.

The most likely explanation for the negligible ejecta deposits at high G (large craters) is that most material was ejected at such low velocity that it did not escape the crater. Using high-speed films of an impact into a target with ~60% porosity, Housen *et al.* (1999) reported a maximum ejection speed of about 19 m/s, with most material having a speed of only a few m/s. At these speeds, most material would land within the crater bowl in a 500G experiment (or in a multi-kilometer crater on a porous asteroid).

In materials like dry sand that have low or moderate porosity and a high crushing strength, if most ejecta were to land within the transient crater, the end result would be only a slight depression[9] or a mound, such as those produced in deeply buried explosions. That is an effect of bulking in those materials. Significant craters are produced in the present experiments because of the large volume created by permanent compaction of pore spaces. Evidence of

compaction can be seen in Figure 13, which is an image derived from a computed tomography (CT) scan of a crater produced at 500G in a target with 60% porosity (Housen *et al.* 1999). The scan was obtained by carefully removing a cylindrical core (centered on the impact point) of material following the impact. The diameter of the core was somewhat larger than the crater, but small enough to allow the CT beam to penetrate the core. The image shows the density of the material in a vertical slice through the crater. Darker shades represent higher densities. The profile of the crater is somewhat irregular due to an unavoidable small disturbance of the target surface while removing the sample core. The image shows a dark region below the crater center, i.e. an area of high relative density, undoubtedly due to compaction of the target material during the impact event.

[Figure 13]

VI. CONCLUDING REMARKS

Craters and ejecta blankets in porous targets form quite differently than in the geological materials typically studied in the lab. Consider, for example, a typical cohesive soil with low or moderate porosity, e.g. less than about 35%. In such a material, the crater forms by shearing and ejection of material along the bowl of the expanding transient crater. Significant ejecta blankets are formed as material is launched to positions outside the crater rim. Housen *et al.* (1983) showed that, for a sequence of increasingly larger craters, the ejecta are deposited relatively closer to the impactor, in terms of impactor radii. This happens because material ejected from fixed positions relative to the impactor (i.e. a fixed multiple of impactor radii) have constant ejection velocity and, therefore, constant ballistic range. The ratio of ballistic range to impactor radius decreases as one considers larger events. When the crater size is large enough that a transition is made to the gravity-dominated regime, a remarkable symmetry occurs in which the crater radius and the ballistic range of

---

[9] This was observed in the experiments reported by Schmidt (1992). When the atmospheric pressure was sufficiently high, the crater bowl was reduced to a minor depression, presumably because there was very little

ejecta both move relatively closer to the impactor in such a way to make the ejecta blankets for all gravity-dominated craters geometrically similar.

Crater formation in highly porous targets proceeds quite differently. Rather than shearing and ejection, much of the crater volume is formed by permanent compaction of the target material. Some material is ejected, as in the less porous cases described above. In fact, the same arguments regarding ejecta should apply. That is, the ejection velocity of material should be constant at positions that are a fixed multiple of impactor radii away from the impact point. Therefore, starting with very small craters and proceeding toward larger ones, ejected material should be deposited closer and closer to the impactor. This behavior was observed in the centrifuge tests. That is, the low-G experiments (small craters on an asteroid) dispersed their ejecta more widely than craters formed at higher accelerations. However, a major departure from the non-porous case occurs when the crater size is large enough such that the transition is initiated into the gravity regime. In the porous case, the ballistic range of ejecta continues to decrease (relative to the impactor radius) so that most of the ejecta lands within the crater. This material does not refill the crater because of the volume created by permanent compaction. Therefore, rather than displaying geometrically similar ejecta blankets in the gravity-regime, craters formed in highly porous materials exhibit essentially no ejecta blankets.[10]

The crater size at which ejecta blankets disappear depends on the velocities of ejected material. Presumably, the lower the ejection speeds, the smaller the crater size at which most ejecta land entirely within the crater. The high porosity of our targets is undoubtedly the reason that ejecta velocities are low.

---

permanent compaction of the sand.

[10] One could argue that, even though the mass of ejecta is small, the ejecta deposits for gravity-dominated craters in porous materials are still geometrically similar. For example, the total mass of ejecta normalized by the crater mass might be a constant value in the gravity regime, which would indicate a kind of geometric similarity. In the present experiments, this would require that the curves shown in Figure 10 flatten out to horizontal lines at large crater sizes. If one could perform experiments at accelerations higher than those reported here, this behavior might indeed be observed.

This explanation contrasts with that provided by Asphaug *et al.* (1998) whose numerical simulations showed that high porosity caused an increase in ejection velocities. There are two differences between their calculations and our experiments. First, their SPH particles were hard spheres, and therefore did not allow for the significant compaction that occurred in our experiments. They do not have significant energy dissipation mechanisms. Compaction of pore spaces is a significant energy sink that contributes to target heating, and may cause a reduction in ejection velocity. Second, the size scale of the pore spaces relative to the impactor may be important in determining how the impact shock propagates through the target (Menikoff 2001, Barnouin-Jha *et al.* 2002). Relatively large pore spaces, like those used in the numerical simulations, severely scatter the shock wave, producing high ejection velocities in the simulations.

Some insight into the effect of pore size on crater size can be gained from experiments conducted in sands having various grain sizes relative to the impactor. Figure 14 shows the scaled crater radius (π_R) versus π_2 from experiments reported by Schmidt (1980) and Cintala *et al.* (1999). These results show that crater size is not affected by the size of the sand grains (and pore spaces), at least for cases where the ratio of impactor diameter to grain diameter is larger than 2. Sand, of course, does not allow for significant compaction during an impact. Hence, Figure 14 does not definitively address the question of how crater and ejecta blanket formation depend on porosity size scale. This question will be addressed in future experiments.

[Figure 14]

The results from our experiments can be used to determine the conditions under which ejecta blankets should or should not form around craters on small bodies. Figure 15 shows an example application to the largest craters observed on asteroids Eros, Ida and Mathilde, and the Martian satellites Deimos and Phobos. The surface gravity of each object, along with the diameter of the largest crater on the body, gives a value of gD. If a bulk porosity is assumed for each body, the data in Figure 11 can be used to estimate the mass ratio of ejecta that

should apply in each case. Ranges of bulk porosity were obtained from Flynn *et al.* (1999), Veverka *et al.* (1999), Wilson *et al.* (1999), Britt and Consolmagno (2000) and Wilkinson *et al.* (2001). Each object in Figure 15 is represented by a shaded region that spans the range of estimated porosity. The value of gD for the largest crater was then used along with the curves[11] shown in Figure 11 to plot the expected mass ratio for a given porosity. Mathilde's exceptionally high porosity and large value of gD together produce a low value for the ejecta mass ratio. The large craters on the other objects shown in Figure 15 could be expected to exhibit significant ejecta. This is consistent with the fact that the large craters on Mathilde do not exhibit noticeable ejecta blankets.

[Figure 15]

It is important to keep in mind that the ejecta mass ratio is scale dependent (i.e. it depends on gD). Therefore ejecta blankets should also be absent around large craters on porous bodies even larger than Mathilde. Smaller bodies, where both g and the size of the largest crater are less than for Mathilde, should eject relatively more material (although the ejecta may escape from small asteroids).

ACKNOWLEDGMENTS

This work was supported by NASA Contract NASW-0007 under the Planetary Geology & Geophysics Program.

[11] These curves are reproduced in Figure 15 as light gray lines and are labeled by their value of gD in cgs units.

REFERENCES

ASPHAUG, E., OSTRO, S.J., HUDSON, R.S., SCHEERES, D.J. AND W. BENZ 1998. Disruption of kilometer-sized asteroids by energetic collisions. *Nature*, 393, 437-440.

.ASPHAUG, E., ET AL??? 2002. Asteroid interiors????. Submitted to *ICARUS*.

BARNOUIN-JHA, O., AND P.H. SCHULTZ 1998. Lobateness of impact ejecta deposits from atmospheric interactions. *J. Geophys. Res.*, **103**, 739-756.

BARNOUIN-JHA, O.,S., CINTALA, M.J. AND D.A. CRAWFORD 2001. Investigating the effects of shock duration and grain size on ejecta excavation and crater growth. *Lunar Planet. Sci. Conf. 33*, Abstract 1738 (CDROM).

BRITT, D.T., YEOMANS, D. HOUSEN, K. AND G. CONSOLMAGNO 2002. Asteroid porosity and structure. Submitted to *ICARUS*.

BRITT, D.T. AND G.J. CONSOLMAGNO S.J. 2000. The porosity of dark meteorites and the structure of low-albedo asteroids. *ICARUS*, **146**, 213-219.

CHAPMAN, C.R., DAVIS, D.R. AND R. GREENBERG 1977. Asteroid fragmentation processes and collisional evolution NASA TM X-3511, 72-73.

CHAPMAN, C.R AND W.J. MERLINE 1999. Cratering on Mathilde. *ICARUS*, **140**, 28-33.

CINTALA, M.J., HEAD, J.W. AND L. WILSON 1979. The nature and effects of impact cratering on small bodies. In *Asteroids* (T. Gehrels, ed.), Univ. Arizona Press, Tucson, Ariz., 579-600.

CONSOLMAGNO, G.J. AND D.T. BRITT 1998. The density and porosity of meteorites from the Vatican collection. *Meteoritics Planet. Sci.*, **33**, 1231-1240.

DAVIS D. R. AND E.V. RYAN 1990. On collisional disruption: Experimental results and scaling laws. ICARUS 83, 156-182.

DIENES, J.K. AND J.M. WALSH 1970. Theory of impact: Some general principles and the method of Eulerian codes. In *High-Velocity Impact Phenonena* (R. Kinslow, ed.), Academic Press, New York.

GREENBERG, J.M. 1986. Fluffy comets. *Asteroids, comets, meteors II; Proc. Int. Meeting,* Uppsala, Sweden, June 3-6, 1985, 221-223.

FUJIWARA, A., KADONO, T. AND A. NAKAMURA 1993. Cratering experiments into curved surfaces and their implication for craters on small satellites. *ICARUS*, **105**, 345-350.

FLYNN, G.J. 1994. Interplanetary dust particles collected from the stratosphere: Physical, chemical, and mineralogical properties and implications for their sources. *Planet. Space Sci.*, **42**, 1151-1161.

FLYNN, G.J., MOORE, L.B. AND W. KLÖCK 1999. Density and porosity of stone meteorites: Implications for the density, porosity, cratering, and collisional disruption of asteroids. *ICARUS*, **142**, 97-105.

Holsapple K. A. 1980. The equivalent depth of burst for impact cratering. *Lunar and Planetary Science XI.*

HOLSAPPLE, K.A., GIBLIN, I., HOUSEN, K., NAKAMURA, A. AND E. RYAN 2002. Asteroid impacts: Laboratory experiments and scaling laws. Submitted to *ICARUS*.

HOLSAPPLE, K.A. AND R.M. SCHMIDT 1980. Theory and experiments on centrifuge cratering. *J. Geophys. Res*, **85**, 235-252.

HOLSAPPLE, K.A. AND R.M. SCHMIDT 1982. On the scaling of crater dimensions II – Impact processes. *J. Geophys. Res*, **87**, 1849-1870

HOLSAPPLE, K.A. AND R.M. SCHMIDT 1987. Point-source solutions and coupling parameters in cratering mechanics. *J. Geophys. Res.* 92, 6350-6376.

HOUSEN, K.R AND K.A. HOLSAPPLE 1999. Scale effects in strength-dominated collisions of rocky asteroids. *ICARUSs.*, **142**, 21-33.

HOUSEN, K.R., SCHMIDT, R.M. AND K.A. HOLSAPPLE 1983. Crater ejecta scaling laws: Fundamental forms based on dimensional analysis. *J. Geophys. Res.*, **88**, 2485-2499.

HOUSEN K.R., HOLSAPPLE, K.A. AND M.E. VOSS 1999. Compaction as the origin of the unusual craters on asteroid Mathilde. *Nature*, **402**, 155-157.

JOHNSON S.W., SMITH, J.A., FRANKLIN, E.G., MORASKI, L.K. AND D.J. TEAL 1969. Gravity and atmospheric pressure effects on crater formation in sand. *J. Geophys. Res.* **74**, 4838-4850.

KIEFFER, S.W. 1975. From regolith to rock by shock. *The Moon*, **13**, 301-320.

LAMBE T.W. AND R.V. WHITMAN 1969. Soil Mechanics, SI version. Wiley & Sons, New York.

LOVE S.G., HORZ F. AND D.E. BROWNLEE 1993. Target porosity effects in impact cratering and collisional disruption. *ICARUS*, **105**, 216-224.

Menikoff, R. 2001. Meso-scale simulations of compaction waves in a granular bed. *23rd Int. Symp. Shock Waves*, Fort Worth Texas, July 22-27, 2001, Paper 5016.

NAKAMURA A., SUGUIYAMA K., AND FUJIWARA A. 1992. Velocity and spin of fragments from impact disruptions I. An experimental approach to a general law between mass and velocity. *ICARUS* 100, 127-135.

NOLAN, M.C., ASPHAUG, E., MELOSH, H.J. AND R. GREENBERG 1996. Impact craters on asteroids: Does gravity or strength control their size?. *ICARUS* 124, 359-371.

O'KEEFE, J.D., STEWART, S.T. AND T.J. AHRENS 2000. Impacts on comets and asteroids, *32nd Div. Planet. Sciences Mtg*, American Astronomical Society, abstract #07.01.

SCHIMMING B.B., HAAS, H.J. AND H.C. SAXE 1965. A comparison of the dynamic and static shear strengths of cohesionless, cohesive and combined soils. Air Force Weapons Lab. Tech Rept. *AFWL TR-65-48.*

SCHMIDT R.M. 1978. Centrifuge simulation of the JOHNIE Boy 500 ton cratering event, *Proc. 9th Lunar Planet. Sci. Conf.*, Vol 3, 3877-3890.

SCHMIDT R.M. 1980. Meteor Crater: Energy of formation – Implications of centrifuge scaling, *Proc. Lunar Planet. Sci. Conf. 11th*, Vol 3, 2099-2128.

SCHMIDT R.M. 1992. Experiments to investigate atmospheric effects on crater size, *Lunar Planet. Sci. Conf. 23rd*, 1221-1222.

SCHMIDT, R.M., HOLSAPPLE, K.A. AND K.R. HOUSEN 1986. Gravity effects in cratering. *Def. Nuc. Agency Rept.* DNA-TR-86-182.

SCHULTZ, P.H. 1982. Atmospheric effects on impact cratering efficiency. *Lunar. Planet. Sci. XIII*, 694-695.

SCHULTZ, P.H. AND O.S. BARNOUIN 1994. Atmospheric containment of crater growth. *Lunar. Planet. Sci. XXV*, 1213-1214 (abstract).

SCHULTZ, P.H., AND D.E. GAULT 1979. Atmospheric effects on Martian ejecta emplacement, *J. Geophys. Res.*,**84**, 7669-7687.

SCHULTZ, P.H., ANDERSON, J.L.B. AND J.T. HEINECK 2002. Impact crater size and evolution: Expectations for deep impact. *Lunar Planet. Sci. Conf. XXXIII*, abstract #1875 (CD ROM).

SIRONO, S. AND J.M. GREENBERG 2000. Do cometesimal collisions lead to bound rubble piles or to aggregates held together by gravity? *ICARUS*, **145**, 230-238.

STEWART, S.T. AND T.J. AHRENS 1999. Porosity effects on impact processes in solar system materials. *Lunar Planet. Sci. XXX*, abstract # 2020 (CD ROM).

VEVERKA, J., THOMAS, P., HIRCH, A., CLARK, B., BELL, J.F., CARCICH, B., JOSEPH, J., MURCHIE, S., IZENBERG, N., CHAPMAN, C., MERLINE, W., MALIN, M., MCFADDEN, L. AND M. ROBINSON 1999. NEAR encounter with asteroid 253 Mathilde: Overview. *ICARUS*, **140**, 3-16,

WATSON, W.W. 1978. Letter on the porosity of asteroids. *Minor Planet Bull.*, **5**, 32.

WILKISON, S.L., ROBINSON, M.S., THOMAS, P.C., VEVERKA, J., MCCOY, T.J., MURCHIE, S.L., PROCKTER, L. AND D. YEOMANS 2001. The porosity of Eros and the implications for its internal structure. *Lunar Planet. Sci. XXXII*, Abstract 1721 (CDROM).

WILSON, L.L., KEIL, K. AND S.J. LOVE 1999. The internal structures and densities of asteroids. *Meteoritics Planet. Sci.*, **34**, 479-483.

Table 1. Summary of Scaling Results in Strength and Gravity Regimes, (Allowing for a Porosity Effect)

Crater measure	General Non-Dimensional Form (Defines Similarity)	Point Source, Strength Regime (Assuming some Y, ρ characterize the target material)	Point Source, Gravity Regime (Assuming ρgh >> any strength measure)
Volume V	$\frac{\rho V}{m} = F\left[\frac{ga}{U^2}, \frac{Y}{\delta U^2}, \frac{\rho}{\delta}, n, \Pi_M\right]$	$\frac{\rho V}{m} = f_{VS}(n)\left(\frac{Y}{\delta U^2}\right)^{\frac{-3\mu}{2}}\left(\frac{\rho}{\delta}\right)^{1-3\nu+\frac{3\mu}{2}}$	$\frac{\rho V}{m} = f_{Vg}(n)\left(\frac{ga}{U^2}\right)^{\frac{-3\mu}{2+\mu}}\left(\frac{\rho}{\delta}\right)^{\frac{2+\mu-6\nu}{2+\mu}}$
Radius R	$R\left(\frac{\rho}{m}\right)^{\frac{1}{3}} = F\left[\frac{ga}{U^2}, \frac{Y}{\delta U^2}, \frac{\rho}{\delta}, n, \Pi_M\right]$	$R\left(\frac{\rho}{m}\right)^{\frac{1}{3}} = f_{RS}(n)\left(\frac{Y}{\delta U^2}\right)^{\frac{-\mu}{2}}\left(\frac{\rho}{\delta}\right)^{\frac{1}{3}-\nu+\frac{\mu}{2}}$	$R\left(\frac{\rho}{m}\right)^{\frac{1}{3}} = f_{Rg}(n)\left(\frac{ga}{U^2}\right)^{\frac{-\mu}{2+\mu}}\left(\frac{\rho}{\delta}\right)^{\frac{2+\mu-6\nu}{3(2+\mu)}}$
Depth h	$h\left(\frac{\rho}{m}\right)^{\frac{1}{3}} = F\left[\frac{ga}{U^2}, \frac{Y}{\delta U^2}, \frac{\rho}{\delta}, n, \Pi_M\right]$	$h\left(\frac{\rho}{m}\right)^{\frac{1}{3}} = f_{hS}(n)\left(\frac{Y}{\delta U^2}\right)^{\frac{-\mu}{2}}\left(\frac{\rho}{\delta}\right)^{\frac{1}{3}-\nu+\frac{\mu}{2}}$	$h\left(\frac{\rho}{m}\right)^{\frac{1}{3}} = f_{hg}(n)\left(\frac{ga}{U^2}\right)^{\frac{-\mu}{2+\mu}}\left(\frac{\rho}{\delta}\right)^{\frac{2+\mu-6\nu}{3(2+\mu)}}$
Ejecta Mass Ratio, M_e/M	$\frac{M_e}{M} = F\left[\frac{Y}{\rho g D}, n, \Pi_M\right]$	$\frac{M_e}{M} = F_s[n, \Pi_M]$	$\frac{M_e}{M} = F_g[n, \Pi_M]$

Table II. Target mixtures and densities

Components			Mixtures (% by mass)					
mat.	ρ	ρ_g	1	2	3	4	5	6
sand	1.6	2.65	100	88	84	77	45	0
perlite	0.1	2.4	0	0	4	11	40	100
fly ash	1.2	2.3	0	12	12	12	15	0
ρ			1.8	1.7	1.5	1.2	0.72	0.11
porosity (%)			32	35	42	53	71	95

Table III. Results of experiments.

shot	material	mix	ρ	n	C/L	G	m	U	D	h	V	Me	Me/M	gD	π2	πR	πv
–	–	–	g/cc	%	–	–	gm	km/s	cm	cm	cc	gm	–	cgs	–	–	–
1786	S	1	1.75	34	CL	508	1.337	1.84	8.26	1.11	31.4			4.12E+06	3.31E-05	4.52	41.11
1785	S	1	1.71	35		509	1.315	1.88	8.26	1.14	30.8			4.12E+06	3.17E-05	4.51	40.05
1780	S/F	2	1.69	35		502	1.326	1.84	9.00	1.39	38.3	21.3	3.30E-01	4.43E+06	3.26E-05	4.88	48.71
1787	S/F	2	1.75	36	CL	503	1.329	1.86	8.76	1.45	38.5	28.7	4.26E-01	4.32E+06	3.21E-05	4.80	50.71
1781	S/F	2	1.70	35	C	504	1.330	1.86	9.30	1.78	40.5	20.5	2.98E-01	4.60E+06	3.21E-05	5.05	51.77
1799	S/P/F	3	1.42	45		1	1.316	1.87	13.22	2.75	110.0	109.0	6.98E-01	1.30E+04	6.30E-08	6.78	118.74
1794	S/P/F	3	1.45	44		10	1.323	1.88	13.10	2.22	116.0	48.7	2.90E-01	1.29E+05	6.25E-07	6.75	126.98
1795	S/P/F	3	1.42	45	CL	10	1.319	1.94	11.14	2.64	98.8	94.1	6.71E-01	1.11E+05	5.97E-07	5.71	106.27
1790	S/P/F	3	1.49	43		50	1.320	1.81	11.46	1.80	83.1	38.1	3.08E-01	5.61E+05	3.35E-06	5.97	93.78
1791	S/P/F	3	1.45	44	CL	50	1.292	1.86	11.66	1.98	88.3	47.1	3.68E-01	5.71E+05	3.16E-06	6.06	99.08
1804	S/P/F	3	1.50	42		239	1.324	1.80	9.52	1.49	48.0	21.0	2.92E-01	2.23E+06	1.63E-05	4.96	54.38
1793	S/P/F	3	1.50	42	CL	240	1.323	1.84	10.14	1.56	54.3	21.3	2.62E-01	2.39E+06	1.56E-05	5.29	61.55
1783	S/P/F	3	1.56	40	C	504	1.339	1.82	9.54	1.53	49.4	18.7	2.42E-01	4.72E+06	3.36E-05	5.02	57.57
1782	S/P/F	4	1.23	52	C	504	1.321	1.85	10.26	1.64	63.7	7.5	9.51E-02	5.07E+06	3.25E-05	5.01	59.31
1805	S/P/F	5	0.69	72		1	1.334	1.94	8.66	5.59	140.0	45.0	4.69E-01	8.50E+03	5.88E-08	3.47	71.99
1797	S/P/F	5	0.70	72	CL	10	1.317	1.85	11.42	4.06	148.0	35.0	3.39E-01	1.14E+05	6.54E-07	4.62	78.43
1792	S/P/F	5	0.79	68	CL	50	1.301	1.82	10.78	3.37	111.0	15.2	1.73E-01	5.32E+05	3.34E-06	4.56	67.40
1820	S/P/F	5	0.73	71	CL	503	1.322	1.85	11.76	1.94	77.7	2.1	3.70E-02	5.80E+06	3.26E-05	4.82	42.92
1788	S/P/F	5	0.78	69	CL	512	1.347	1.84	11.00	1.97	82.4	4.4	6.78E-02	5.53E+06	3.35E-05	4.58	47.73
1811	P	6	0.11	95		10	1.328	1.85	24.80	4.32	680.0			2.43E+05	6.45E-07	5.41	56.34
1810	P	6	0.10	96		50	1.326	1.85	22.40	4.12	454.0			1.10E+06	3.22E-06	4.79	35.62
1813	P	6	0.10	96	CL	50	1.324	1.84	17.00	5.26	371.0	0.3	8.81E-03	8.34E+05	3.26E-06	3.64	29.14
1808	P	6	0.11	96		509	1.333	1.98	11.74	4.87	231.0			5.86E+06	2.85E-05	2.52	18.19
1815	P	6	0.10	96	CL	509	1.319	1.85	11.82	4.51	225.0	0.03	1.31E-03	5.90E+06	3.28E-05	2.52	17.40

Notes: [1] Material designators are S=sand, P=perlite, F=fly ash. The mix designator refers to the recipes shown in Table 1. [2] The C/L flag indicates the use of the cloth ejecta collector (C) and the lid over the test container (L). [3] Shot 1805 was conducted in a vacuum.

FIGURE CAPTIONS

Figure 1. Results of explosive field cratering tests conducted in sand, playa and dry alluvium. All of the craters were generated by spherical high-explosive charges half-buried so that their center was coincident with the target surface. The increase in cratering efficiency of playa with increasing explosive mass is indicative of a strain-rate dependent strength. As discussed in the text, this is thought to be due to the high moisture content of the playa medium. The alluvium, which was quite dry, shows a constant cratering efficiency, which suggests the strength of this material is independent of strain rate.

Figure 2. A 335G centrifuge simulation of an explosive field cratering test. In order to match the similarity requirements, the simulation was conducted at an acceleration of 335G in the same medium (dry alluvium) as the field test. The field test (Stagecoach III) used $2x10^7$ gm (20 tons) of high explosive buried at a depth of 10.4 meters. The resulting crater was 36 m in diameter. The crater profile from the centrifuge test is shown enlarged by the scale factor of 335, as discussed in the text.

Figure 3. The size distribution of the F75 sand and perlite used in the porous target materials.

Figure 4. Quasistatic compressive and tensile strengths of the porous sample materials.

Figure 5. Some of the centrifuge tests used a bowl-shaped lid over the target container in order to assure that all ejecta were collected. The crater profiles shown here demonstrate that the lid did not adversely affect the crater profile at accelerations of 50G and higher. A small effect is observed in the experiments conducted at 10G, undoubtedly the result of ejecta bouncing off the lid and back into the crater.

Figure 6. Profiles that show how crater size and shape depend on acceleration for fixed values of target porosity.

Figure 7. Profiles that show how crater size and shape depend on target porosity for fixed values of acceleration.

Figure 8. Cratering efficiency for impacts in porous materials. The materials with 44% and 77% porosity both show a constant cratering efficiency with a transition to a gravity-dominated regime at large values of π_2. The transition to the gravity regime is consistent with the strength measurements for these materials, as discussed in the text. Cratering efficiency is observed to decrease as target porosity increases.

Figure 9. Craters formed in materials with 44% porosity (left column) and 70% porosity (right column) at three accelerations. High acceleration (large simulated crater diameter) and high porosity both tend to reduce the amount of material ejected beyond the crater rim.

Figure 10. The normalized mass of ejecta steadily decreases as the gravity-scaled crater size increases. This is due to the fact that as the event size increases, more launched material ends up back within the crater.

Figure 11. For a given crater size, the normalized mass of ejecta decreases as target porosity increases. Increasing porosity probably causes a reduction in ejection velocity, so that relatively more material lands inside the crater.

Figure 12. Effect of atmospheric pressure on cratering efficiency. Data for 1G are from Schultz (1992) for impacts into F-140 sand and pumice. The remaining data are from shallowly buried explosions reported by Schmidt (1992). The dependence of cratering efficiency on pressure is strongest for experiments conducted at 1G acceleration.

Figure 13. Result of a computed tomography (CT) scan of a crater produced in the experiments reported by Housen *et al.* (1999). The target had an initial porosity of 60%. This image represents the density of the post-impact material in a vertical plane through the impact point. Darker shades represent regions of higher density. The scan shows a region of enhanced density beneath the crater caused by compaction due to the impact shock.

Figure 14. Crater size for impacts into dry sand show that crater size is insensitive to the size of the sand grains, when the grains are no more than half the size of the impactor.

Figure 15. The mass ratio of ejecta that is expected to apply to the largest observed craters on Mathilde, Eros, Ida and the Martian satellites Deimos and Phobos. A shaded region is shown for each object that covers the range of estimated porosities taken from the literature. The value of surface gravity and largest crater diameter are used, along with the results shown in Figure 11, to plot the ejecta mass ratio that should apply to each object. Two shaded regions are shown for Mathilde that represent different assumptions about the analog type of carbonaceous chondrite material of which Mathile is composed. Because of Mathilde's exceptionally high porosity, it is the only object expected to have a low ejecta mass ratio. This is consistent with the fact that Mathilde's large craters exhibit little evidence of ejecta blanketing.

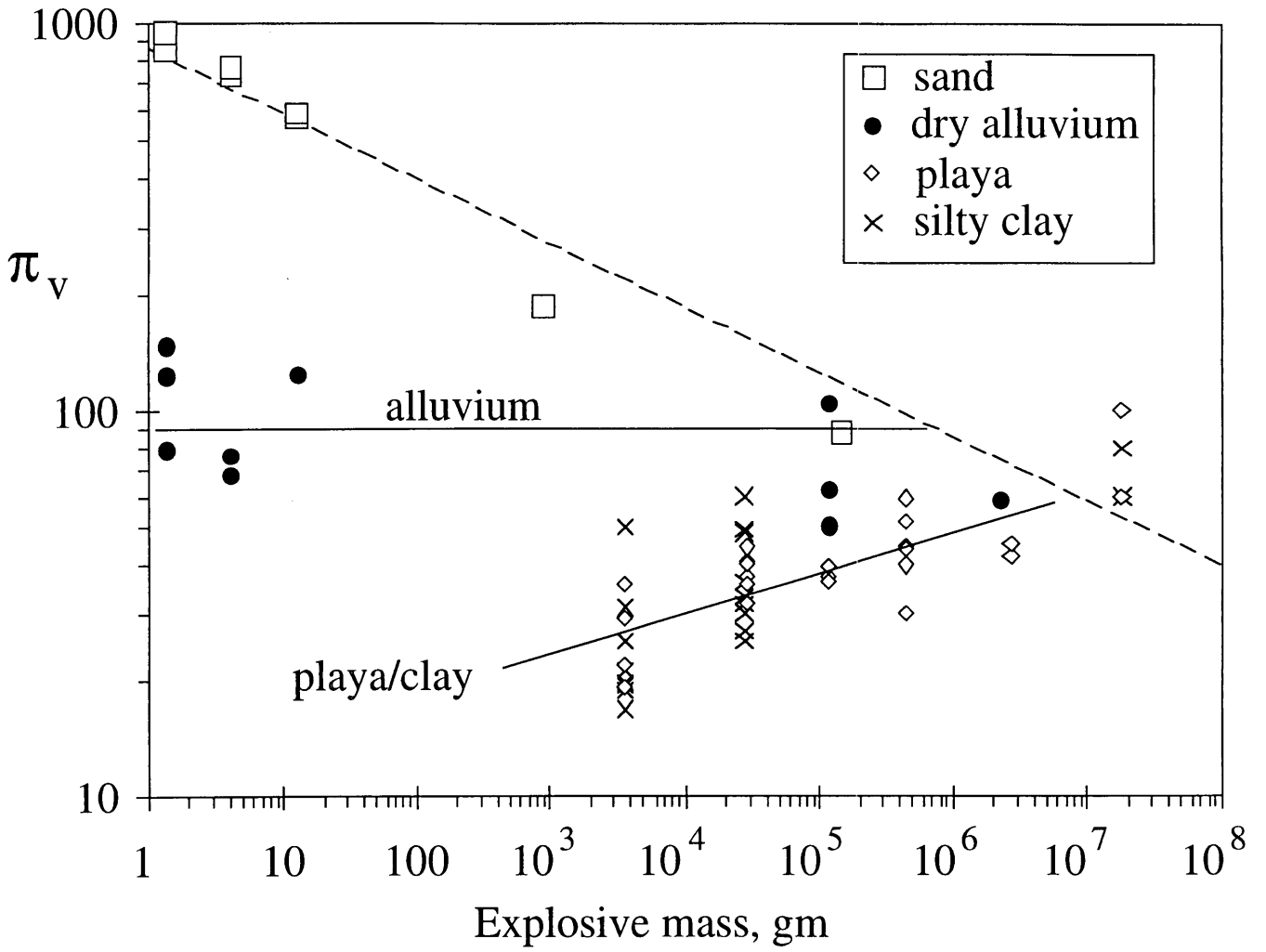

Figure 1. Housen and Holsapple. Impact Cratering on Porous Asteroids.

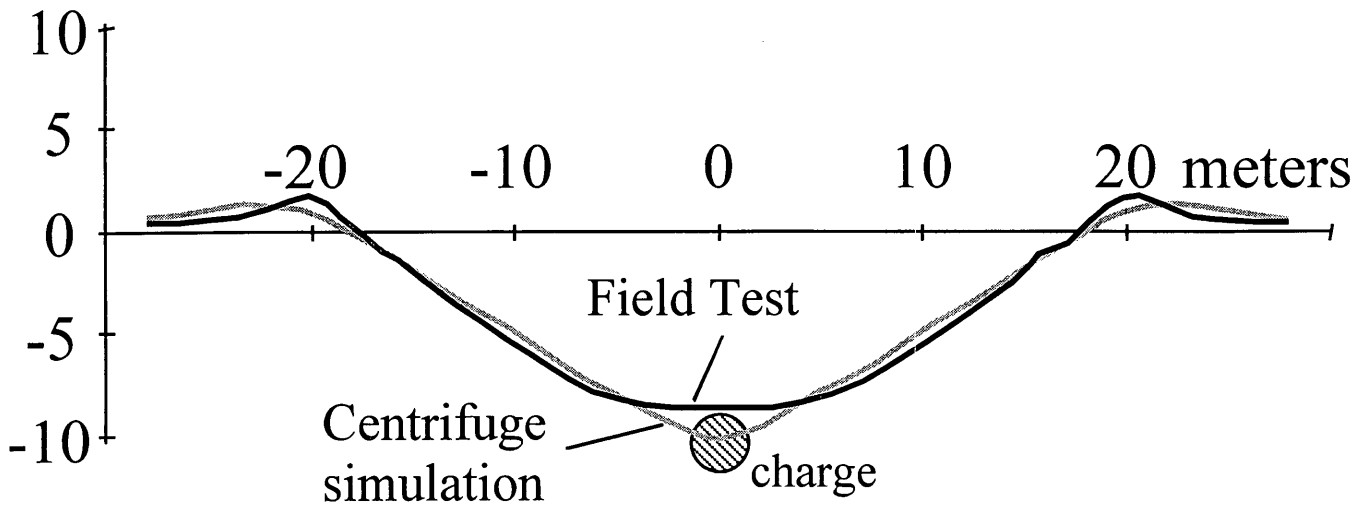

Figure 2. Housen and Holsapple. Impact Cratering on Porous Asteroids.

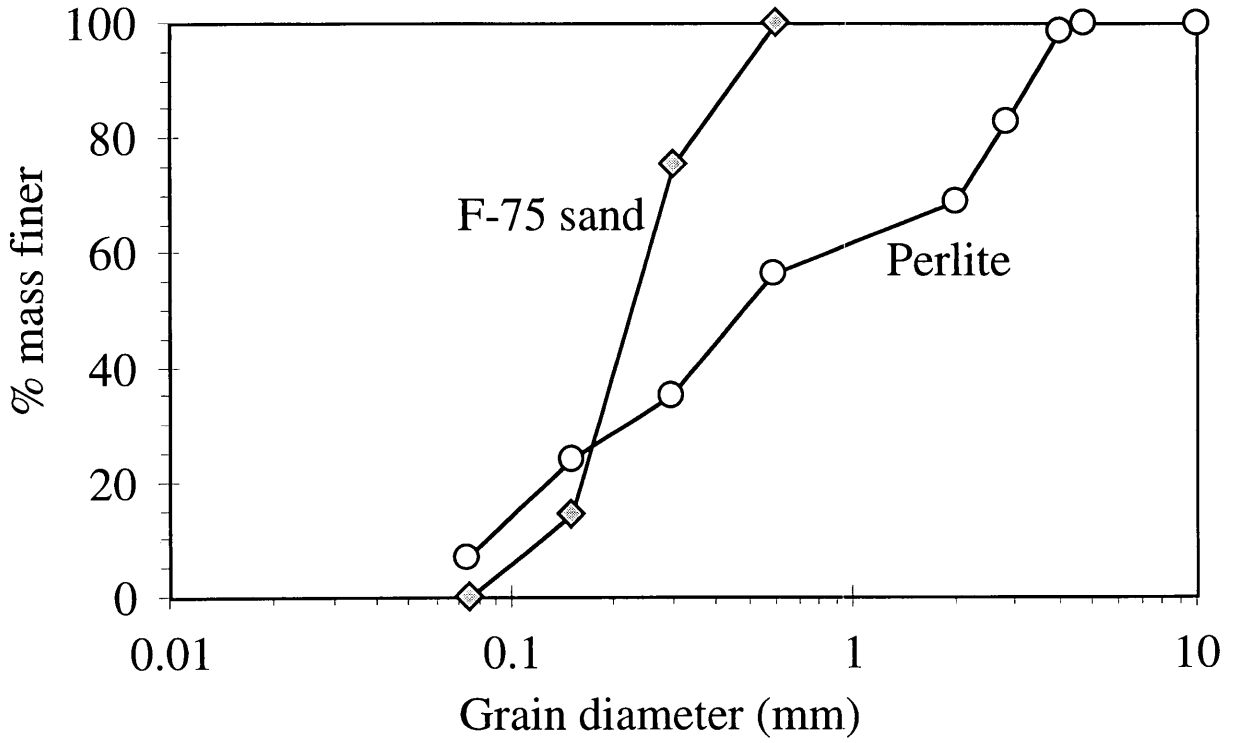

Figure 3. Housen and Holsapple. Impact Cratering on Porous Asteroids.

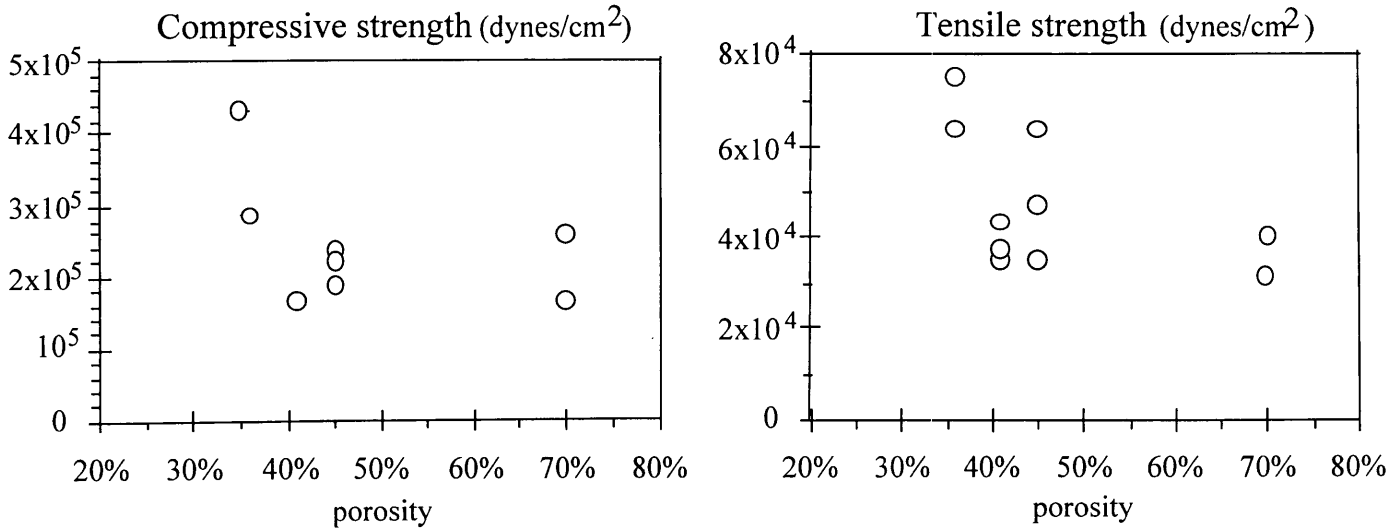

Figure 4. Housen and Holsapple. Impact Cratering on Porous Asteroids.

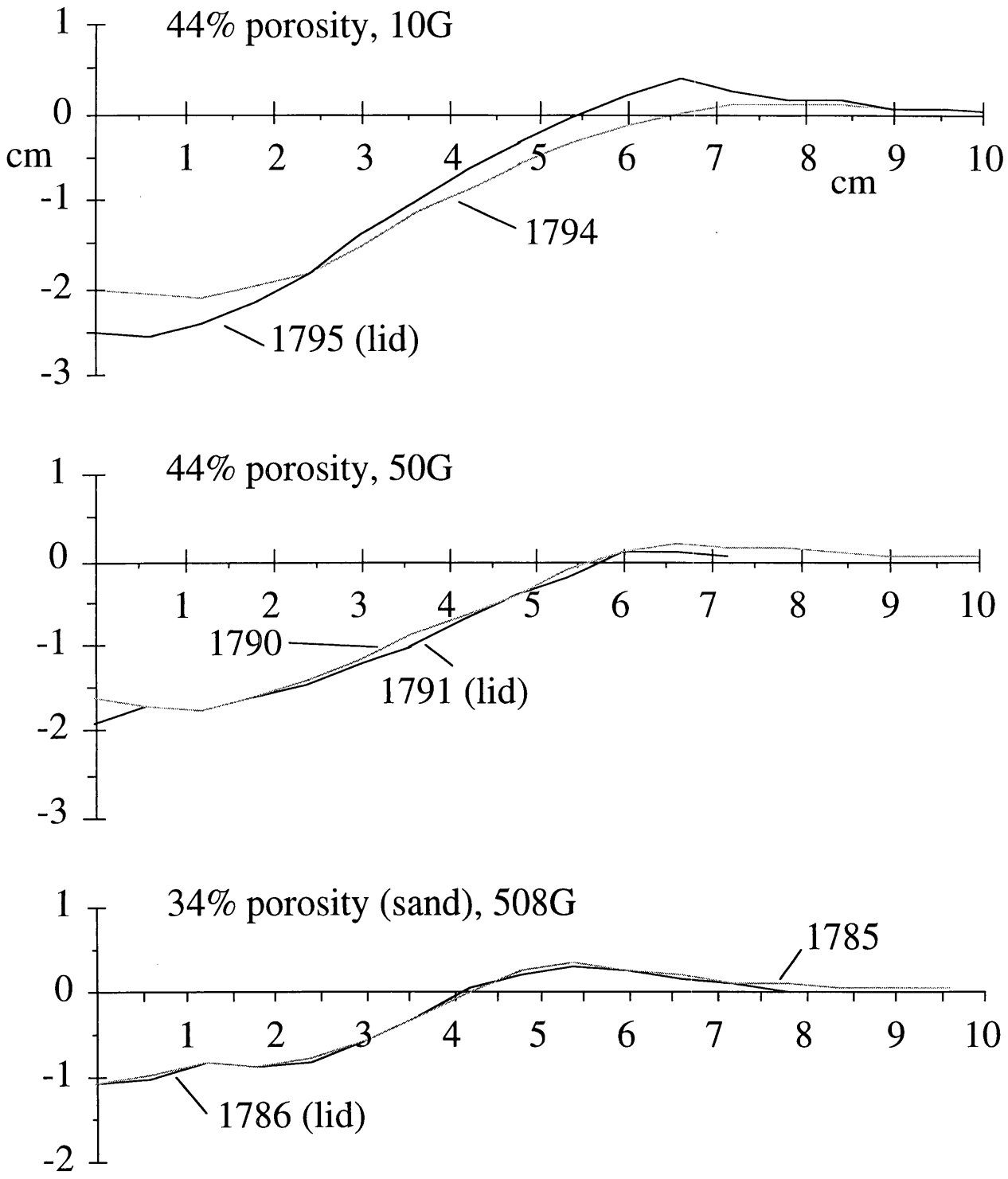

Figure 5. Housen and Holsapple. Impact Cratering on Porous Asteroids.

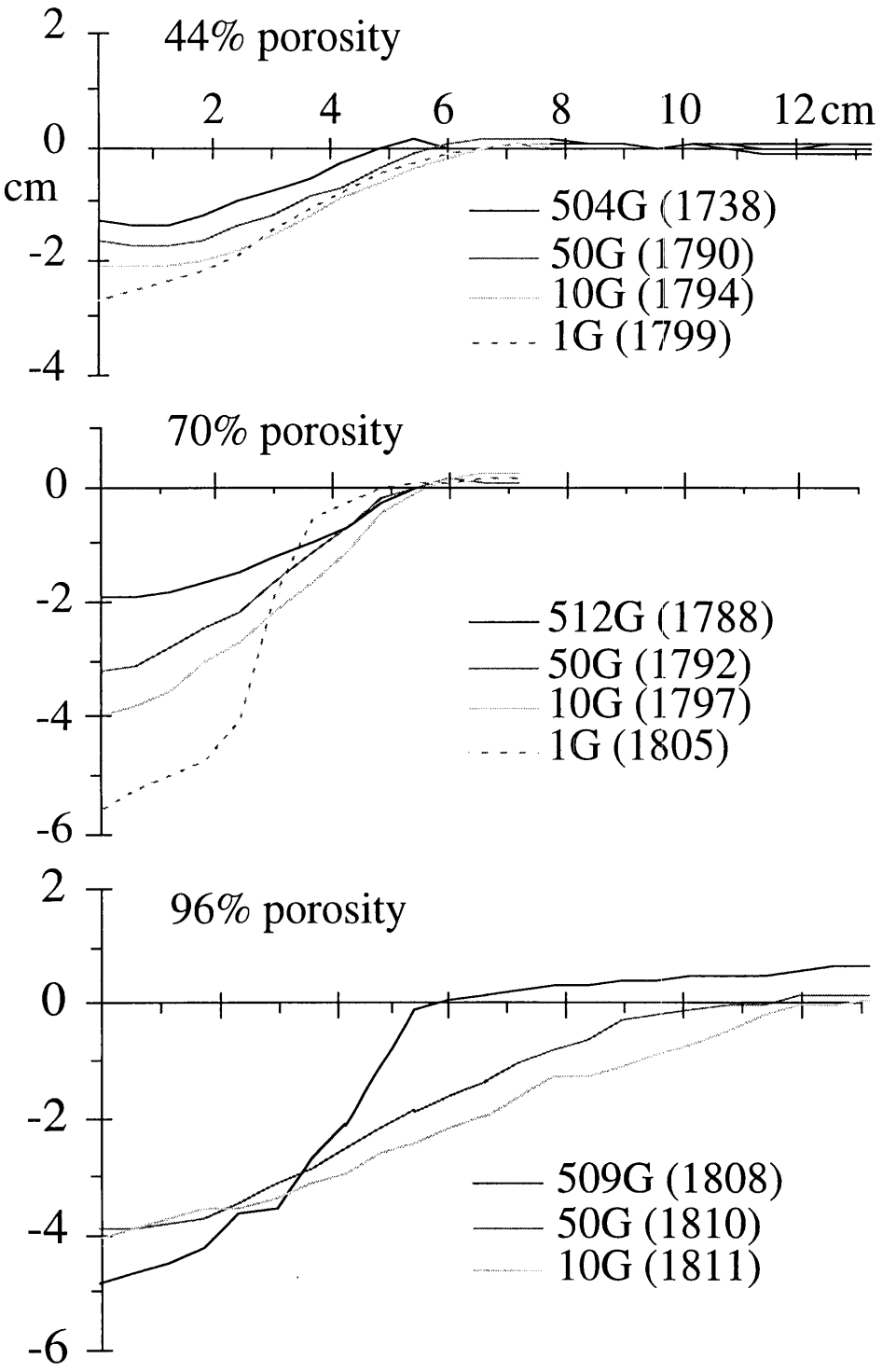

Figure 6. Housen and Holsapple. Impact Cratering on Porous Asteroids.

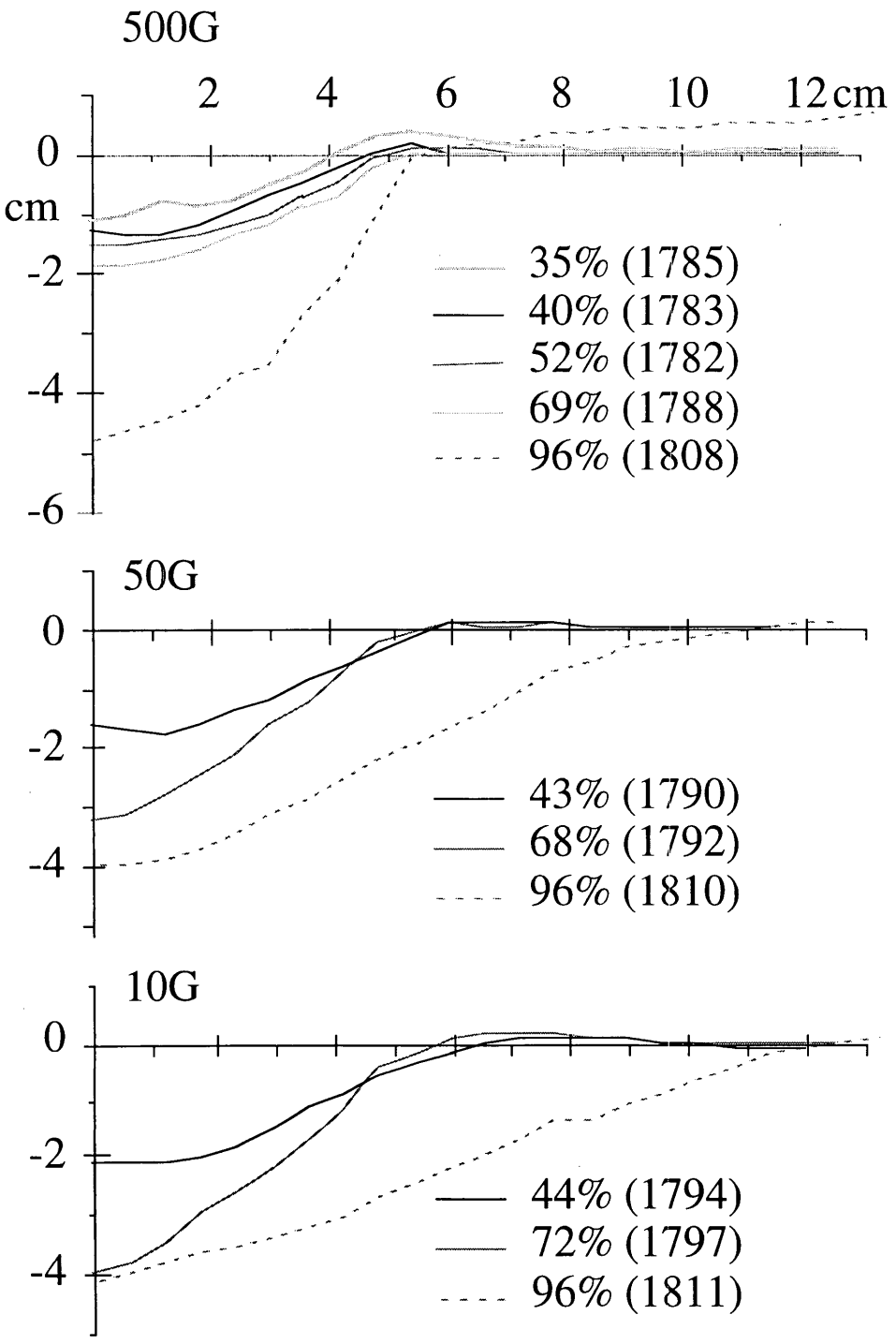

Figure 7. Housen and Holsapple. Impact Cratering on Porous Asteroids.

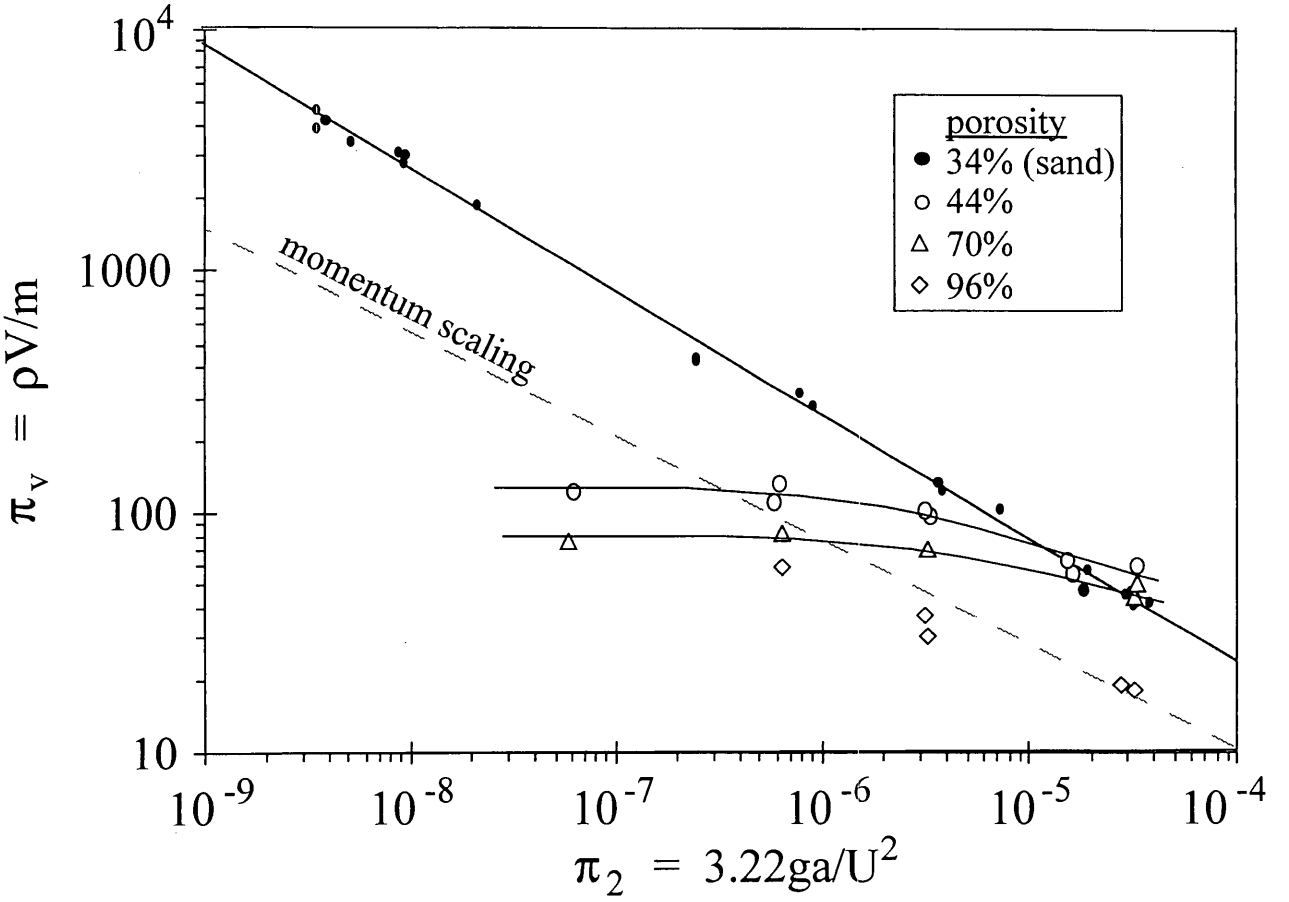

Figure 8. Housen and Holsapple. Impact Cratering on Porous Asteroids.

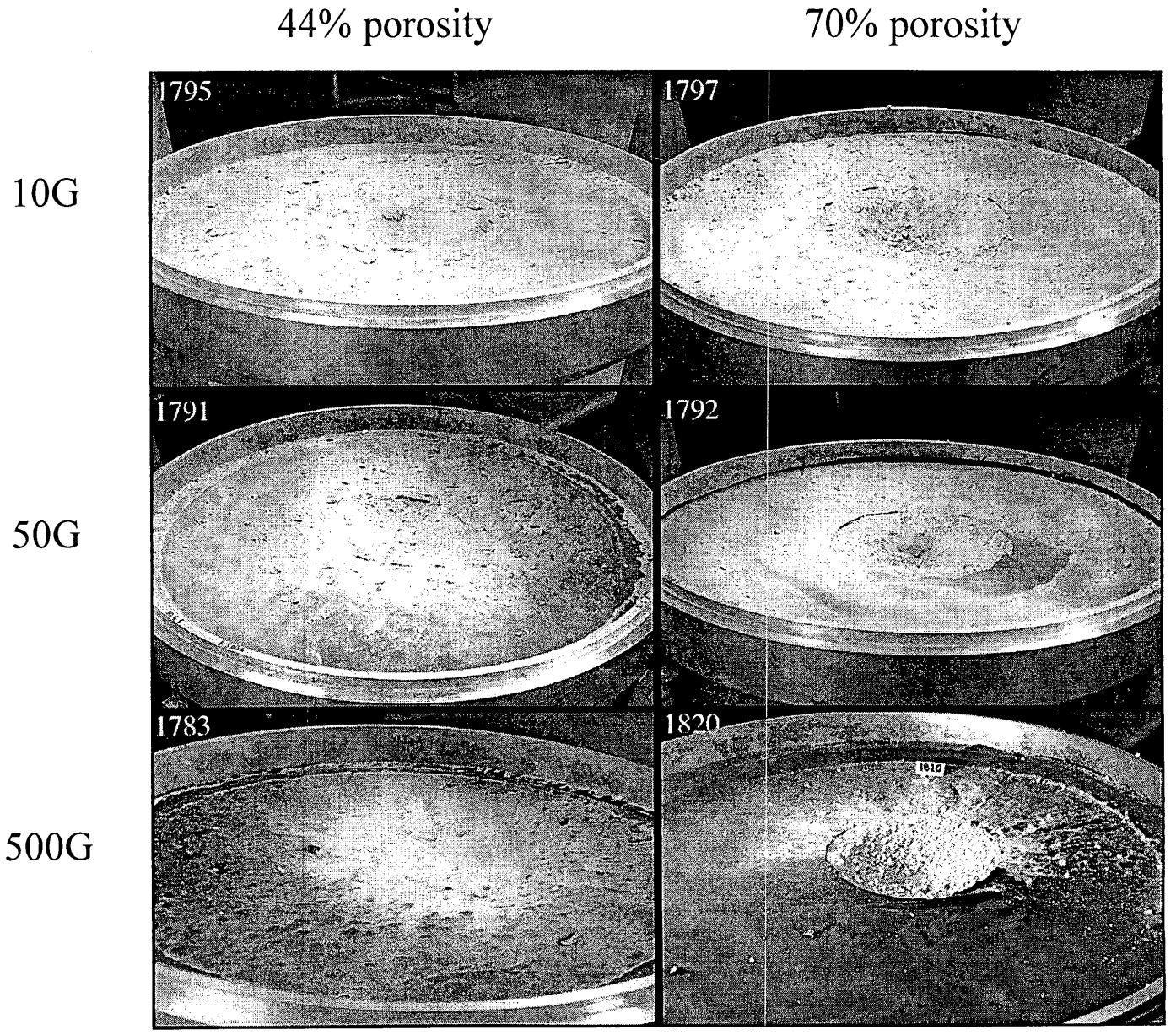

Figure 9. Housen and Holsapple. Impact Cratering on Porous Asteroids.

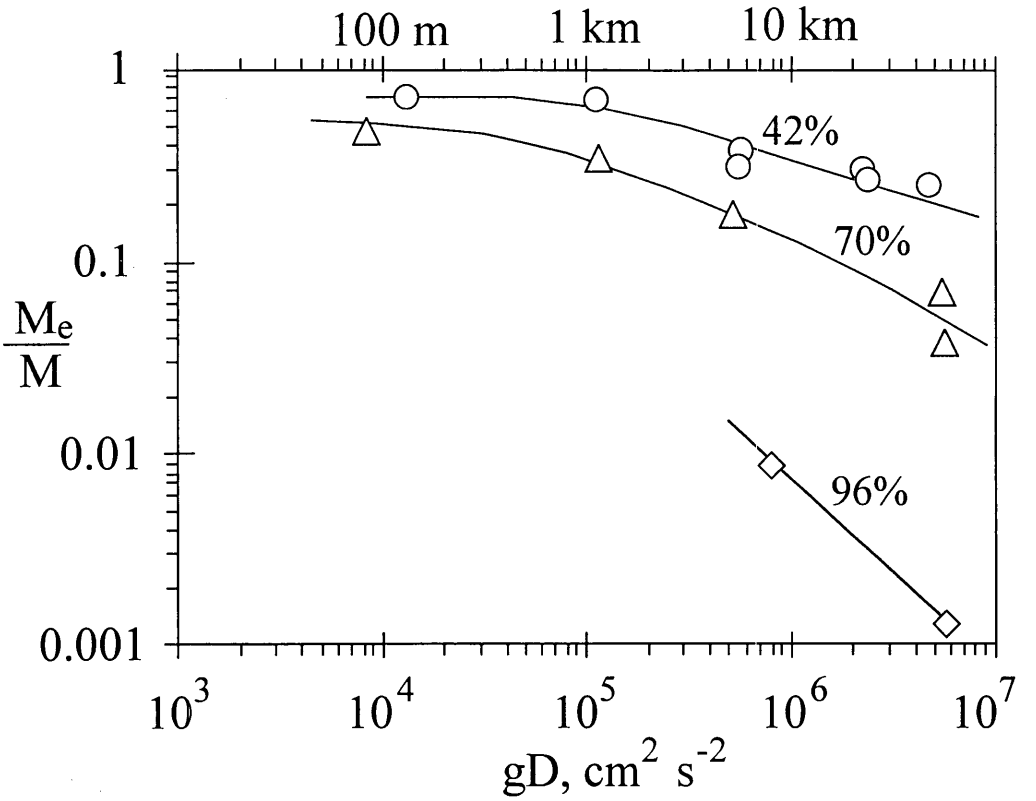

Figure 10. Housen and Holsapple. Impact Cratering on Porous Asteroids.

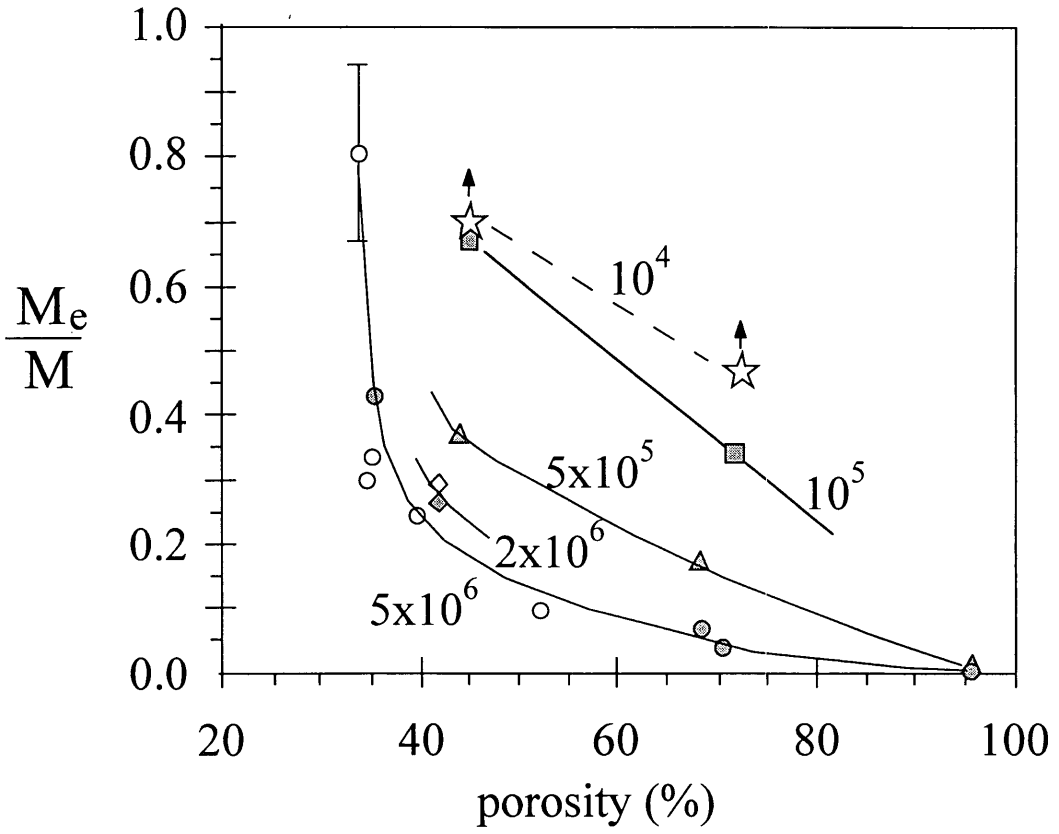

Figure 11. Housen and Holsapple. Impact Cratering on Porous Asteroids.

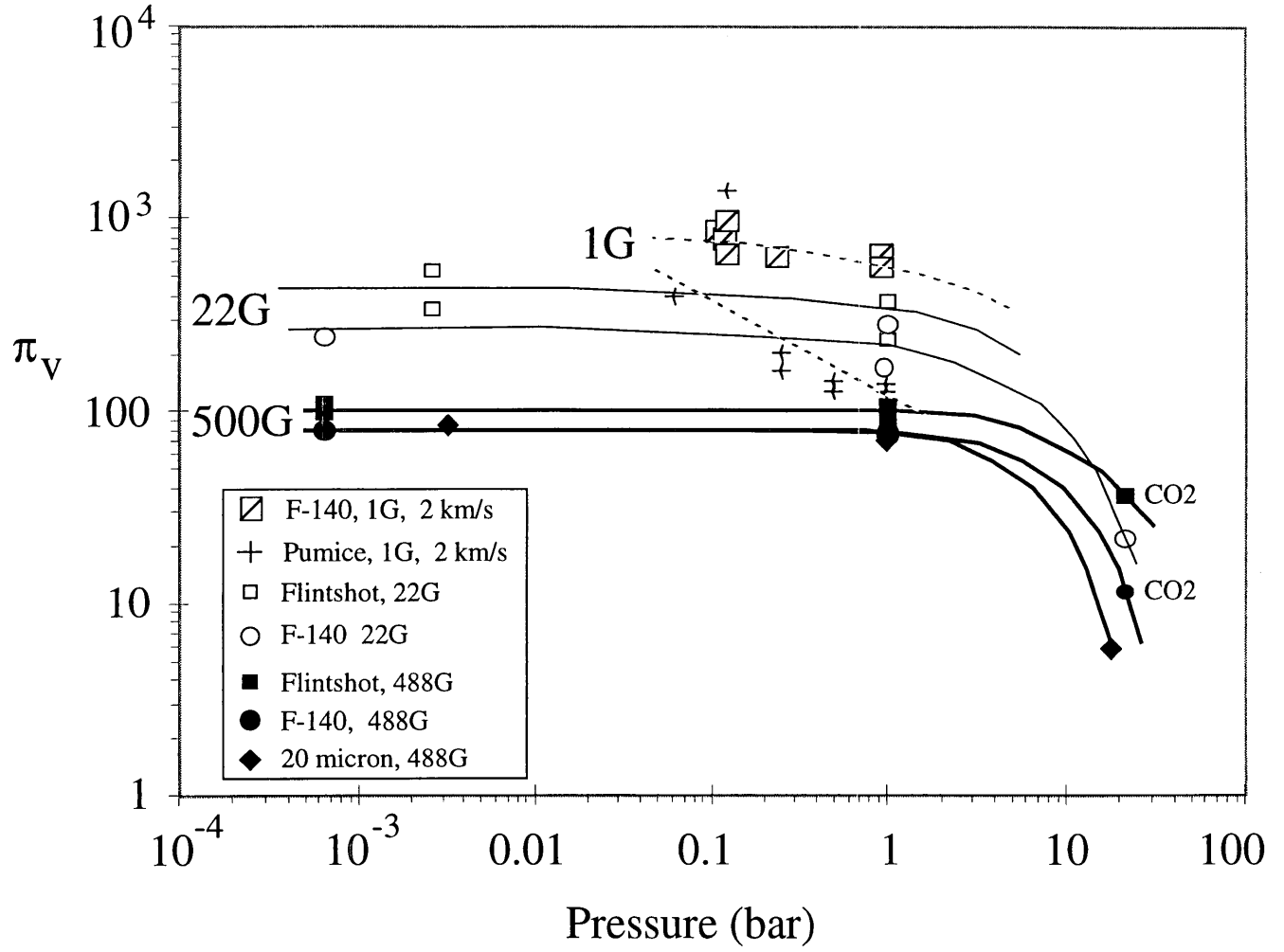

Figure 12. Housen and Holsapple. Impact Cratering on Porous Asteroids.

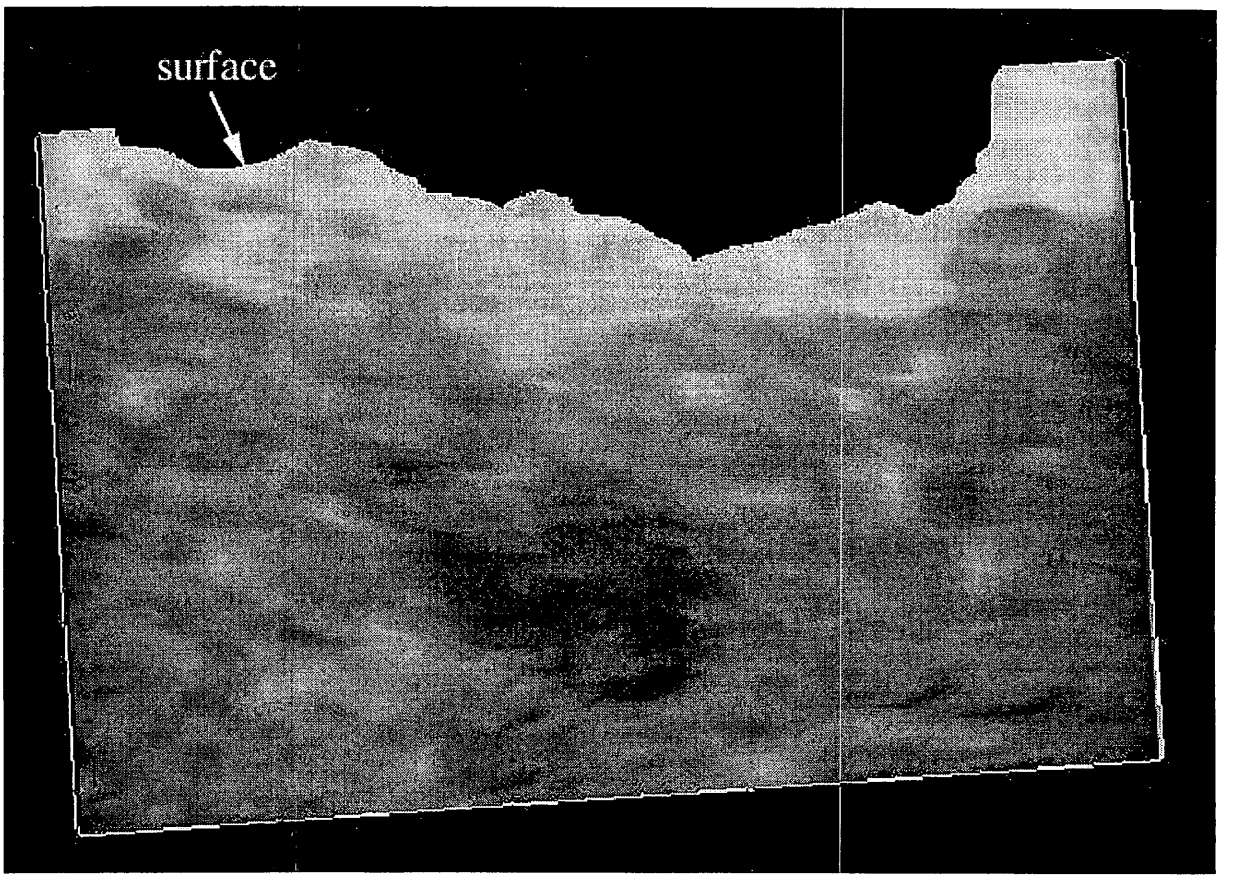

Figure 13. Housen and Holsapple. Impact Cratering on Porous Asteroids.

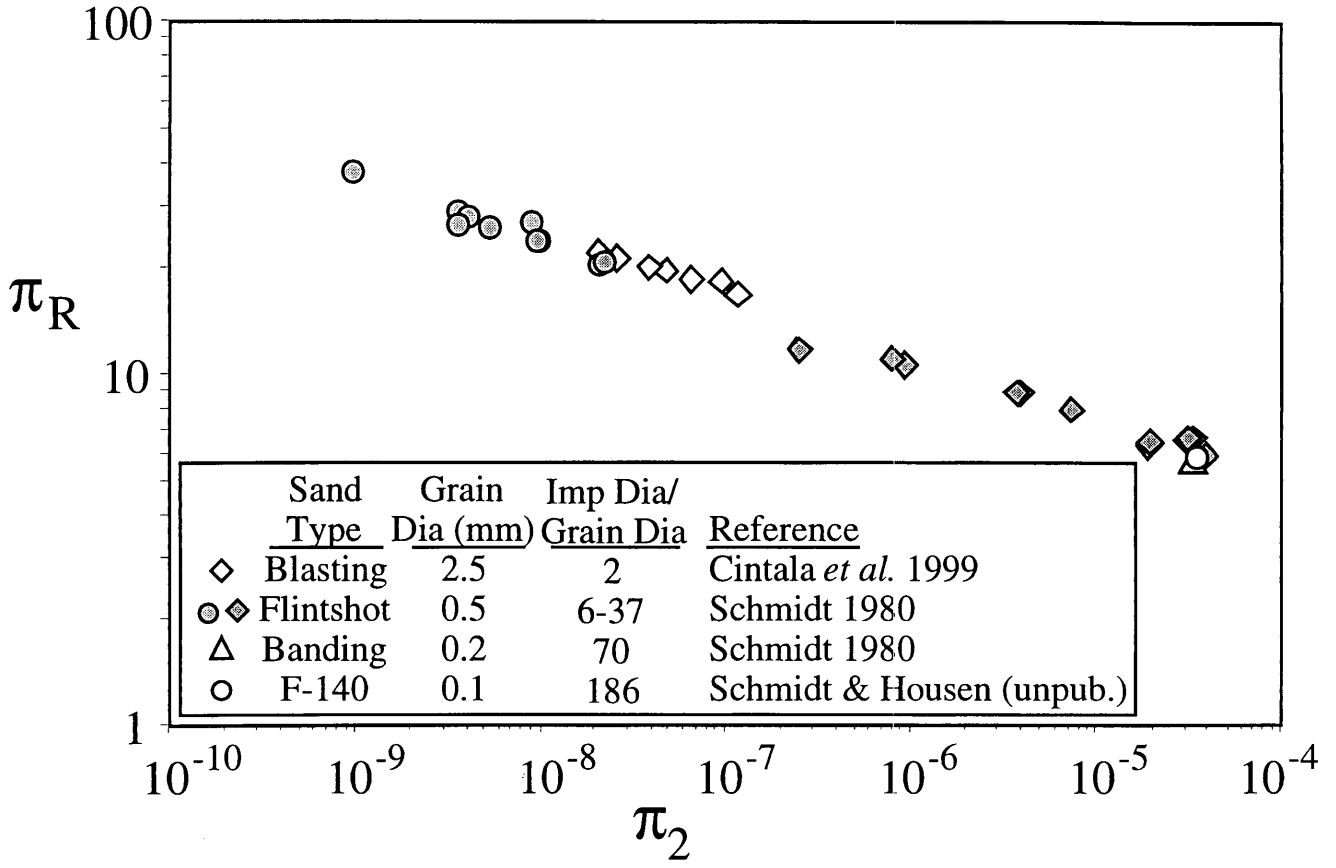

Figure 14. Housen and Holsapple. Impact Cratering on Porous Asteroids.

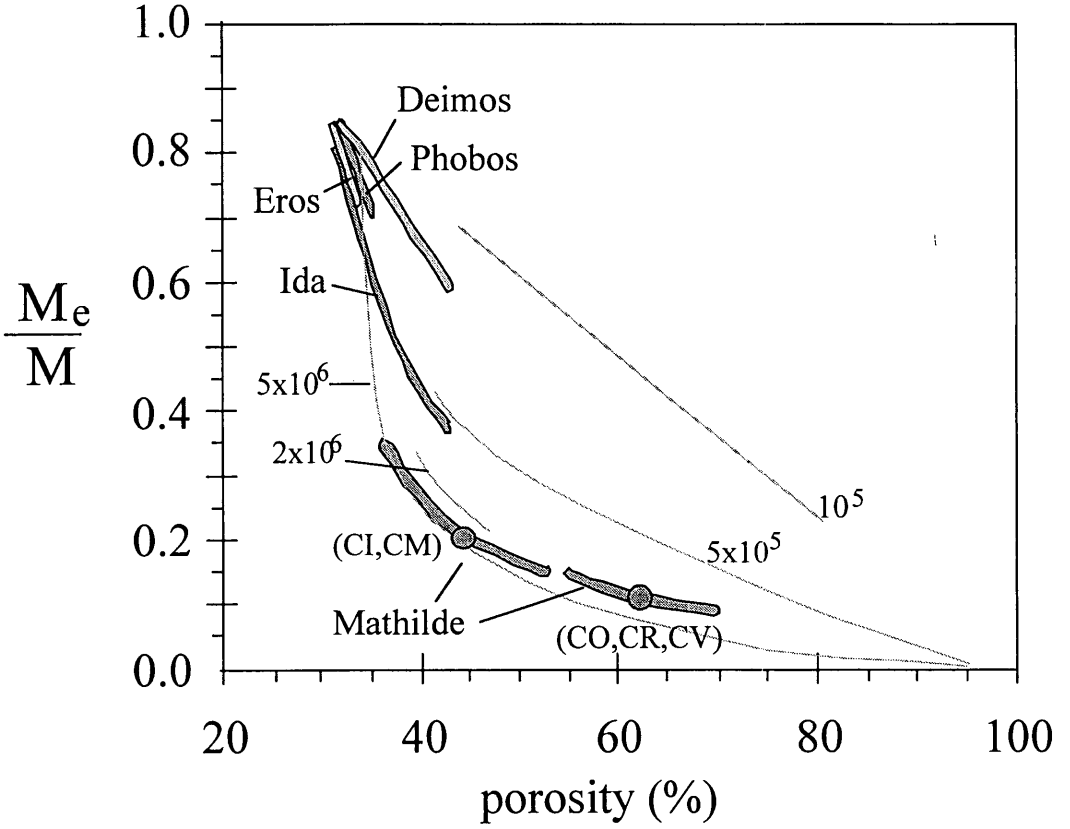

Figure 15. Housen and Holsapple. Impact Cratering on Porous Asteroids.

Slides presented at the 33rd LPSC regarding the strength-gravity transition for impacts in porous materials.

Does gravity scaling apply to impacts on porous asteroids?

Kevin Housen

The Boeing Co., MS 2T-50, P.O. Box 3999, Seattle WA 98124

kevin.r.housen@boeing.com

33rd Lunar & Planetary Science Conference

Houston TX March 11-15, 2002

What determines crater size?

- Gravity is irrelevant! (circa 1970)
- Target strength is irrelevant! (circa 1996)
  - strength diminishes as strain rates decrease
  - shock fractures material ahead of expanding crater
- Strength/gravity transition for porous materials?
  - understand the mechanisms that control crater size
  - need to scale experiments (e.g. Deep Impact)
  - crater/ejecta morphology can be used to infer strength properties.

Strength

- Mohr-coulomb model of shear strength
  - determined by cohesion, Y, and friction angle, ϕ
  - shear strength = $Y + \sigma_n \tan(\phi)$

Fractured ≠ strengthless

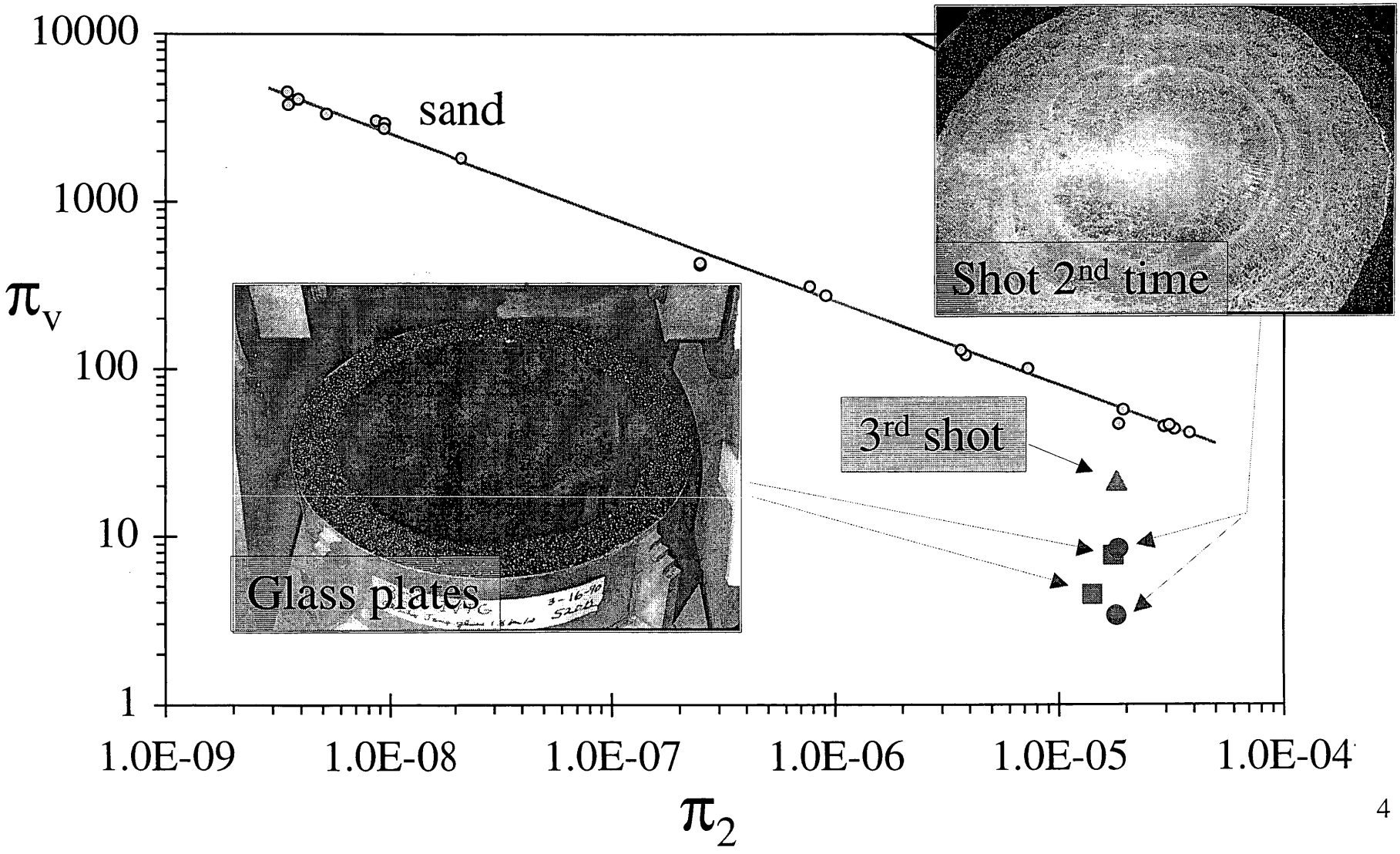

Scaling: simple materials

Cohesion, Y, is independent of size and time scales

π_V = cratering efficiency = $\rho V/m$

π_2 = gravity-scaled size = $3.22ga/U^2$

π_Y = nondimensional strength = $Y/\delta U^2$

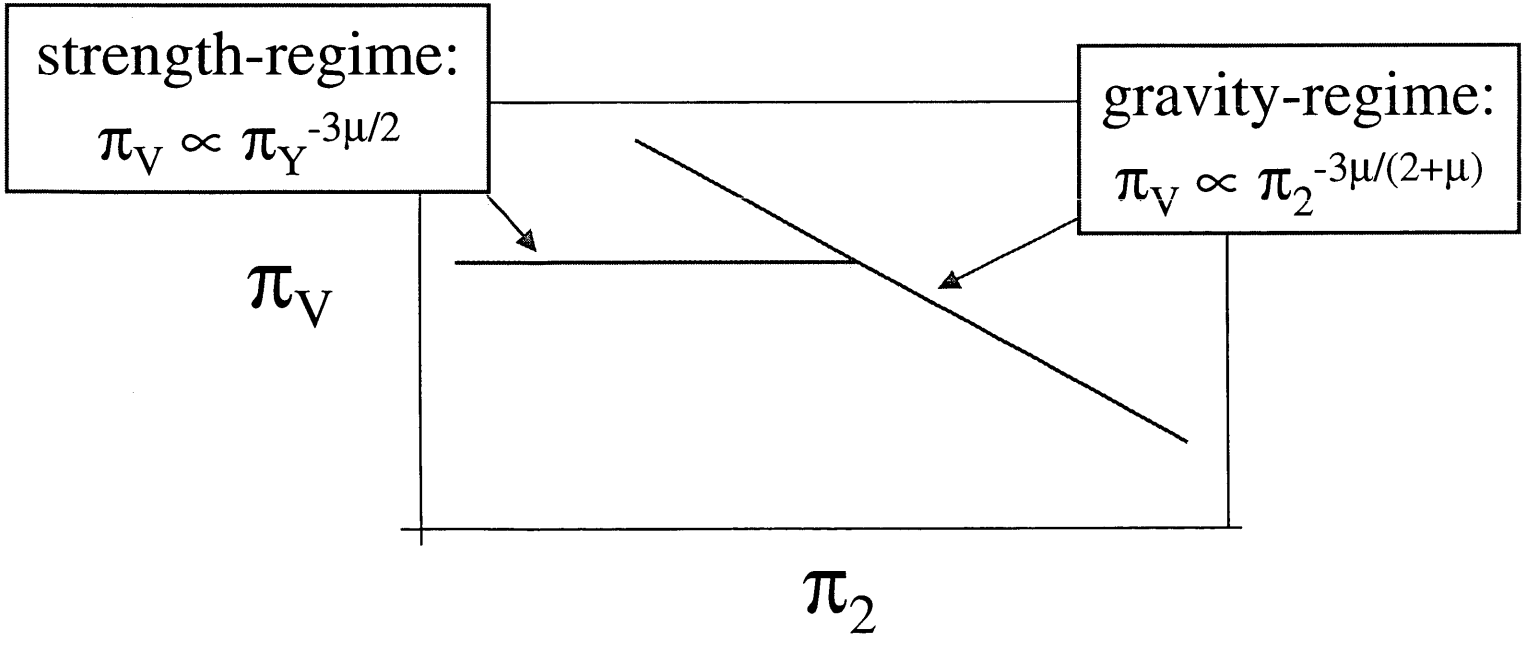

Scaling: rate-dependent materials

If cohesion is rate dependent: $Y = Y_0 \dot{\varepsilon}^{3/\phi}$

ϕ is the usual Weibull exponent

Y_0 is a material property with units of [stress][time]$^{3/\phi}$

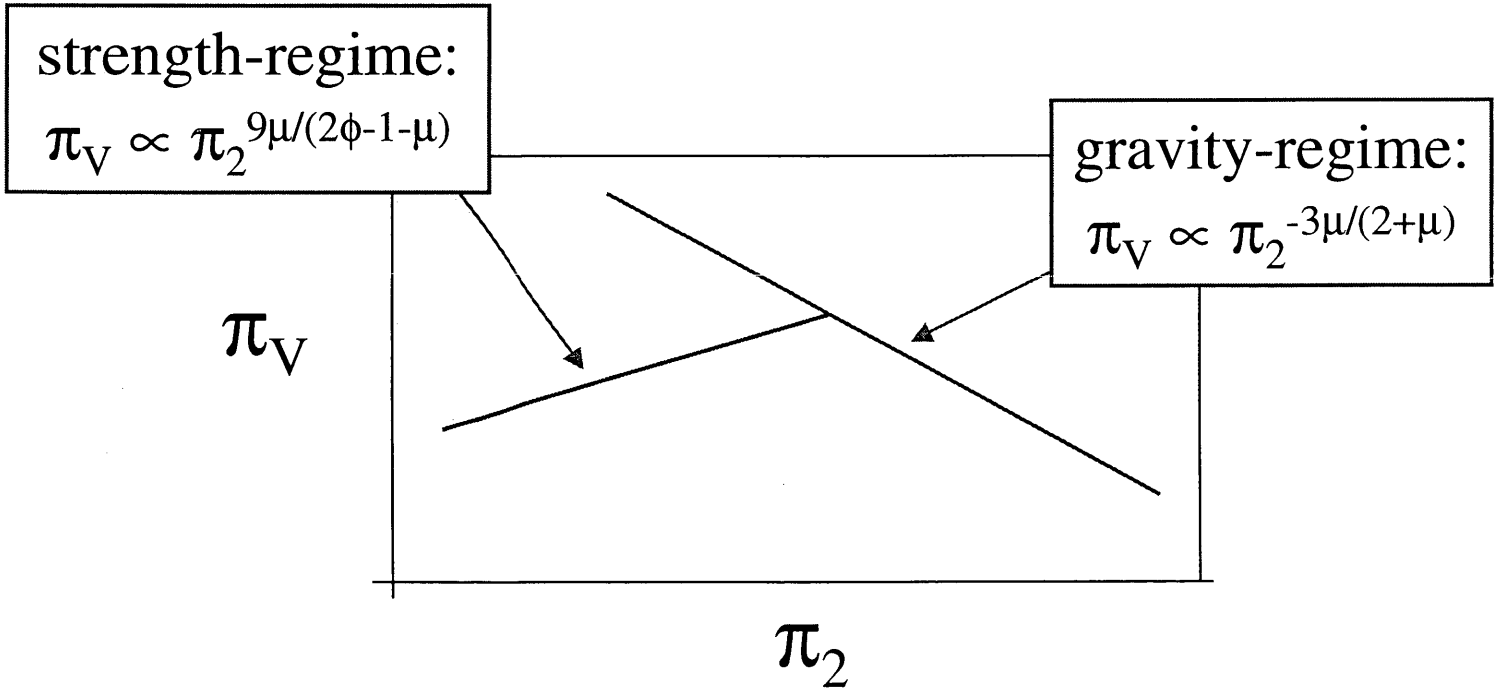

Explosions as a test for rate effects

LPSC 33

- Shallowly buried explosions are good analogs of impact (Oberbeck 1977; Holsapple 1980)
- Field data span a factor of
  - 5×10^7 in energy
  - 330 in size scale

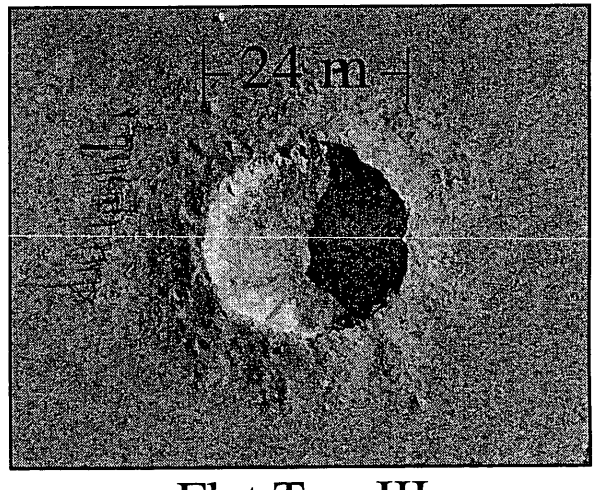

Flat Top-III
40,000 lb TNT

Explosion crater data (1G)

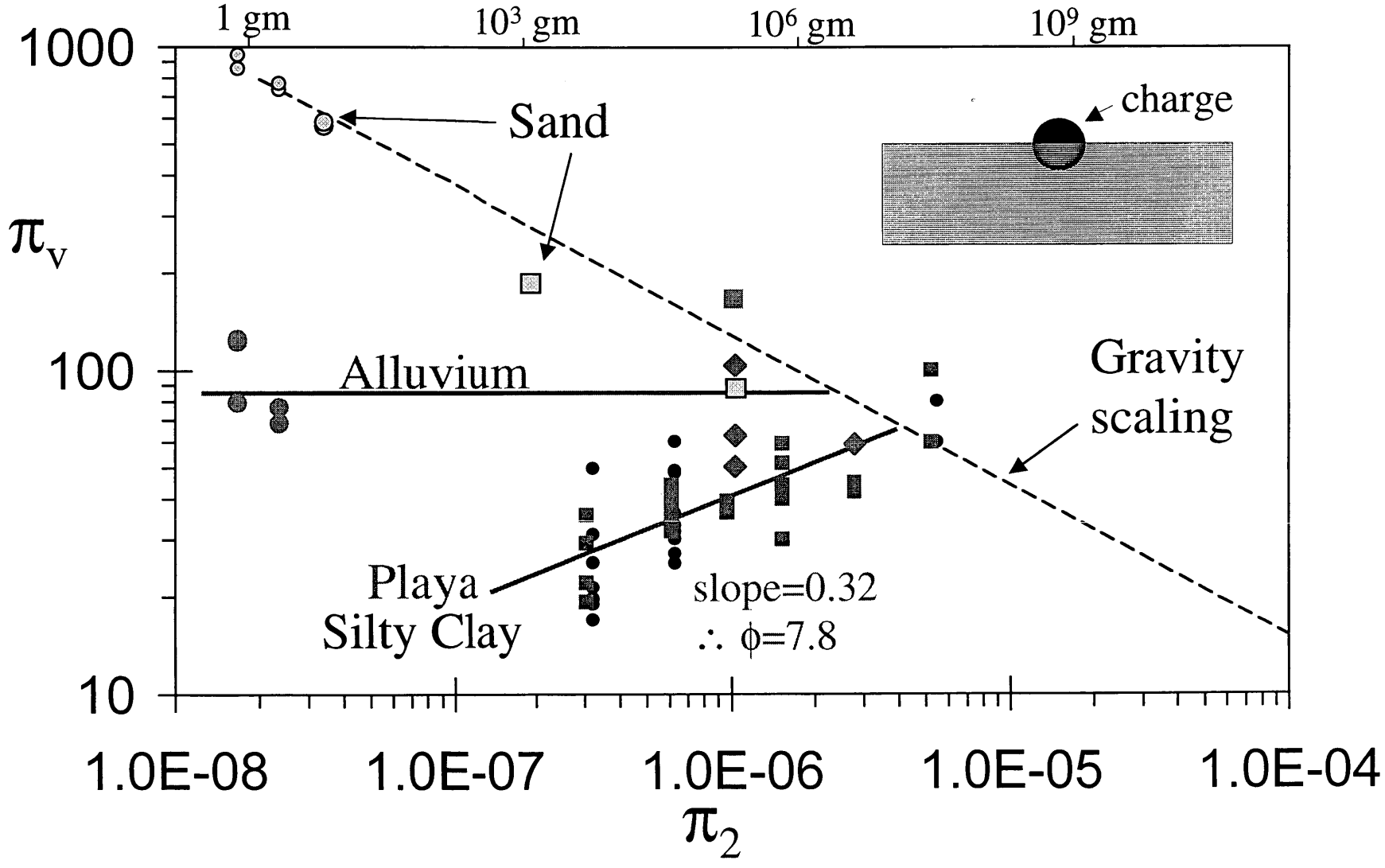

Rate-effects in soils

- Dynamic shear tests on a variety of soils (Schimming et al. 1968)
- Cohesionless soils showed no rate dependence
- Cohesive soils
  - Alluvium
    - showed no rate dependence
    - consistent with explosive field tests that show π_v = constant
  - Silty clays
    - cohesion increases as loading rate increases
    - friction angle = constant

Strain-rate effect in soils

- Moisture is largely responsible for the increase in apparent cohesion at high strain rates.
- Difference between alluvium and playa cratering behavior is probably due to moisture content.

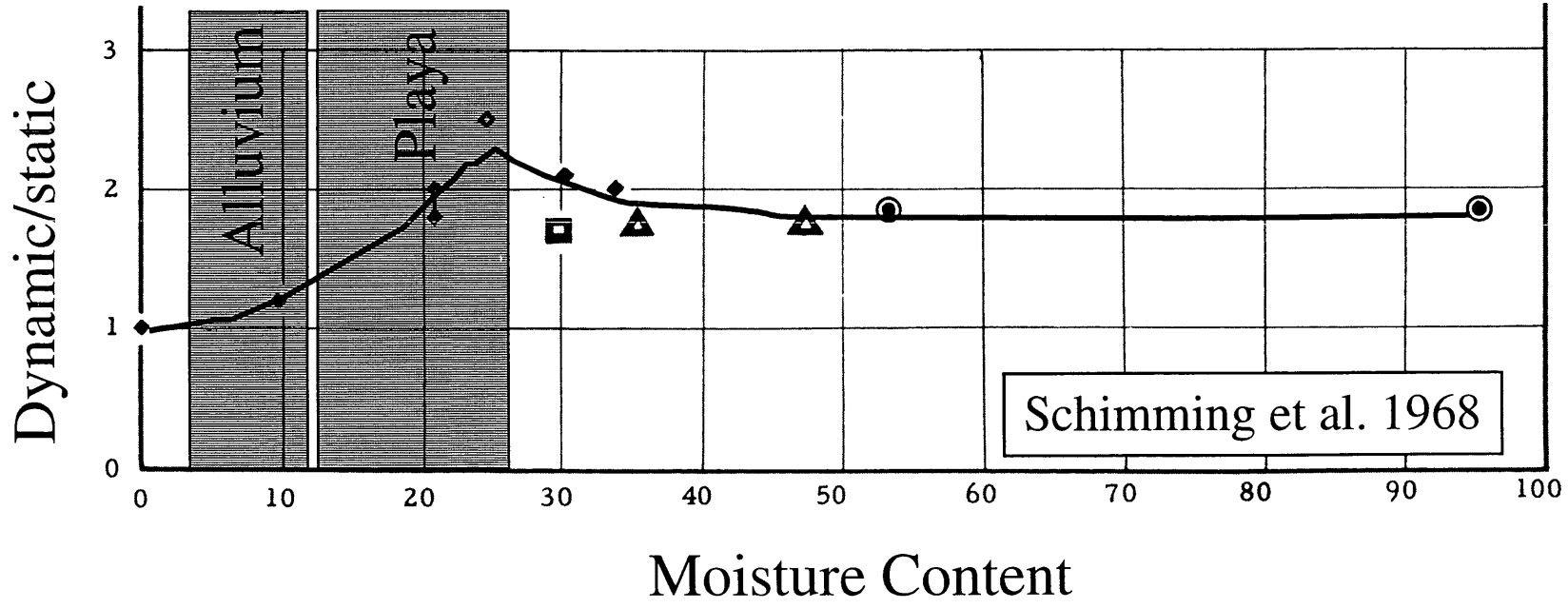

Figure 4.7 Apparent Cohesion Ratio Response for Various Soil-Water Combinations

Centrifuge experiments

- Porous soil
  - porosity = 43%, 70%
  - cohesion ~ 5 kPa
- Terrestrial soils typically have cohesion in the range of 30 -100 kPa.

Centrifuge experiments

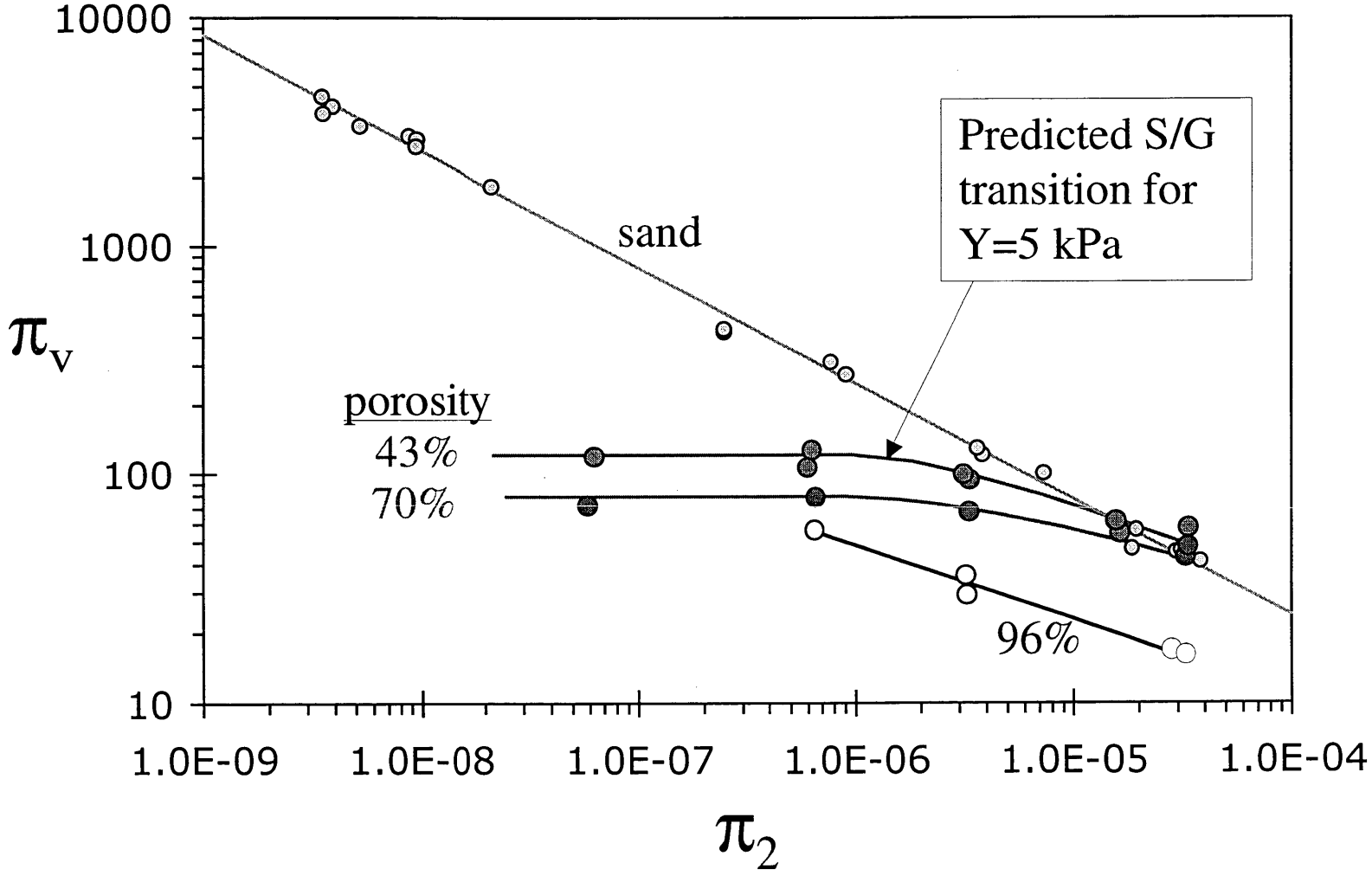

Strength-gravity transition

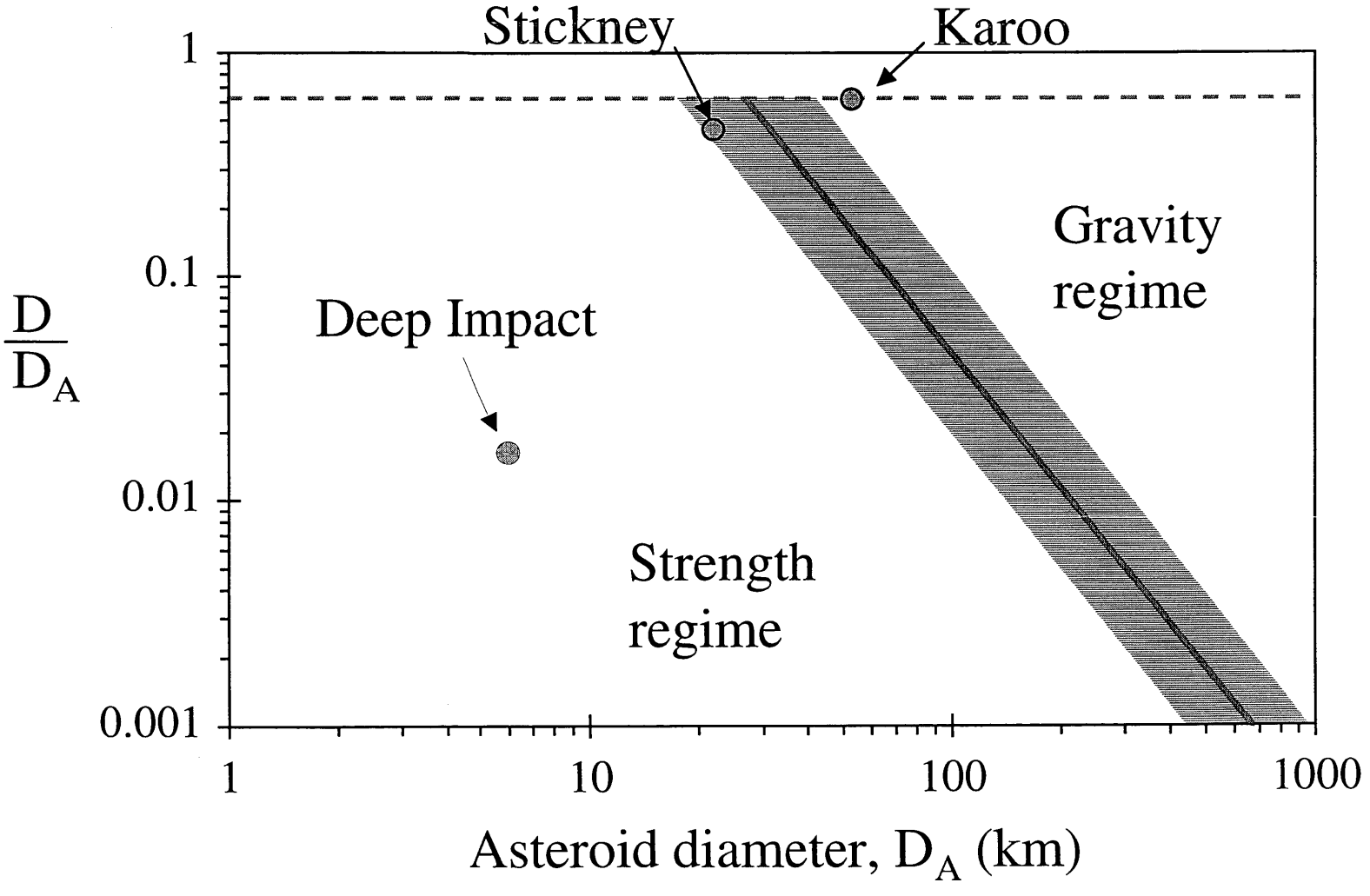

Rate-dependent strength

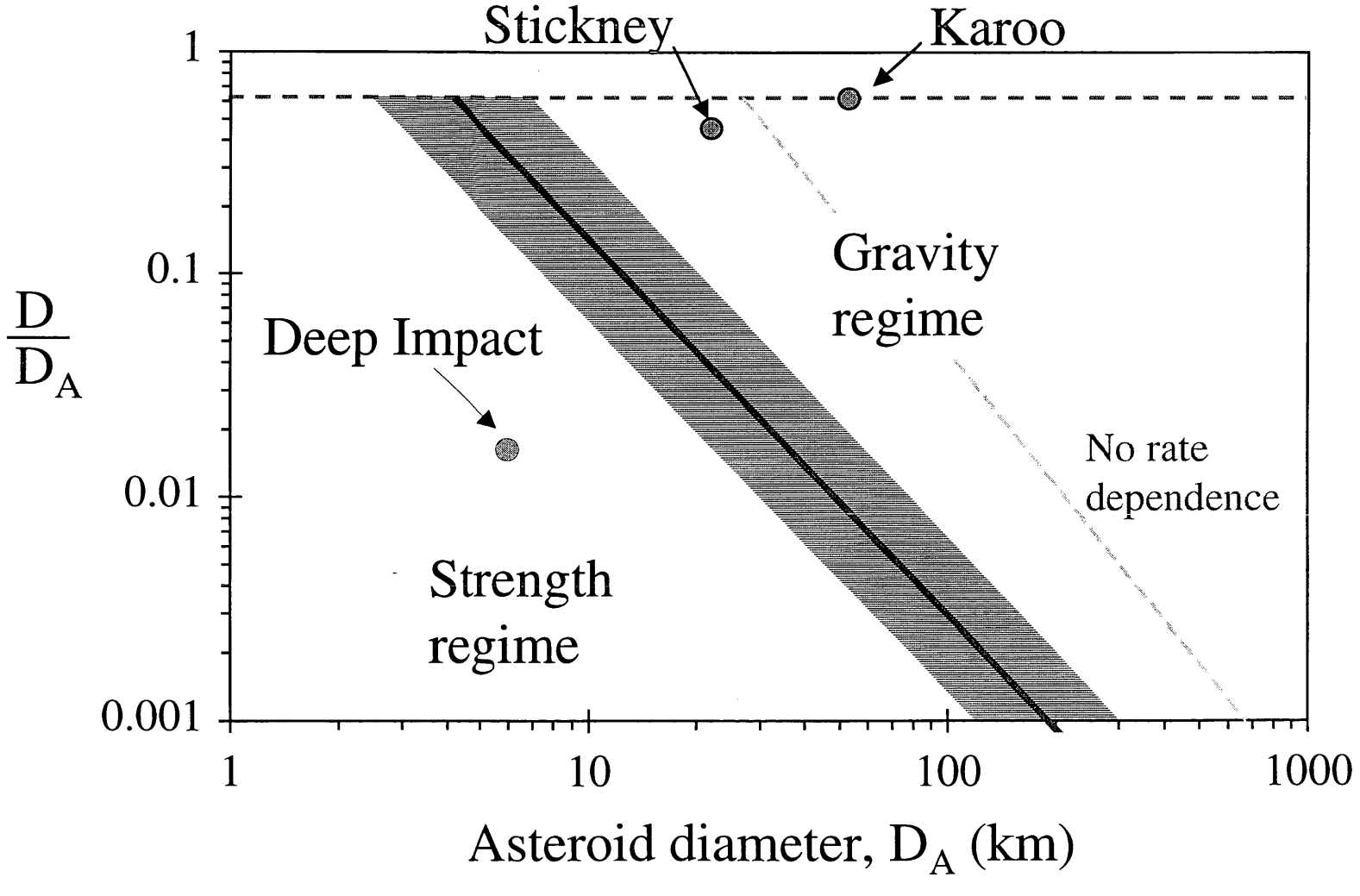

Conclusion

- Fractured materials still have considerable strength in shear.
- We still have a lot to learn about porous materials.
- Dry soils do not show an appreciable dependence of strength on strain rate
- If porous asteroids have strengths comparable to the materials used here, only bodies larger than ~30 km will have any gravity-dominated craters.

TR/IN/190

REPORT DOCUMENTATION PAGE

Form Approved
OMB No. 0704-0188

1. AGENCY USE ONLY (*Leave blank*)	2. REPORT DATE	3. REPORT TYPE AND DATES COVERED
	5/10/2002	Annual report 6/23/01-6/22/02

4. TITLE AND SUBTITLE

Experimental Simulations of Large-Scale Collisions

5. FUNDING NUMBERS

NASW-00007

6. AUTHOR(S)

Kevin R. Housen

7. PERFORMING ORGANIZATION NAME(S) AND ADDRESS(ES)

The Boeing Co.
P.O. Box 3707
Seattle, WA 98124

8. PERFORMING ORGANIZATION REPORT NUMBER

9. SPONSORING/MONITORING AGENCY NAME(S) AND ADDRESS(ES)

NASA Headquarters
New Technology Representative
Attn: Dr. Robert Norwood, Code R
Washington, D.C. 20546

10. SPONSORING/MONITORING AGENCY REPORT NUMBER

11. SUPPLEMENTARY NOTES

This work was sponsored by the NASA Planetary Geology and Geophysics program

12a. DISTRIBUTION/AVAILABILITY STATEMENT

Unlimited

12b. DISTRIBUTION CODE

13. ABSTRACT (*Maximum 200 words*)

This report summarizes research on the effects of target porosity on the mechanics of impact cratering. Impact experiments conducted on a centrifuge provide direct simulations of large-scale cratering on porous asteroids. The experiments show that large craters in porous materials form mostly by compaction, with essentially no deposition of material into the ejecta blanket that is a signature of cratering in less-porous materials. The ratio of ejecta mass to crater mass is shown to decrease with increasing crater size or target porosity. These results are consistent with the observation that large closely-packed craters on asteroid Mathilde appear to have formed without degradation to earlier craters.

14. SUBJECT TERMS			15. NUMBER OF PAGES
Asteroid	Impact		80
Crater	Ejecta		16. PRICE CODE
Porosity	Strength-gravity transition		

17. SECURITY CLASSIFICATION OF REPORT	18. SECURITY CLASSIFICATION OF THIS PAGE	19. SECURITY CLASSIFICATION OF ABSTRACT	20. LIMITATION OF ABSTRACT
UNCLASSIFIED	UNCLASSIFIED	UNCLASSIFIED	SAR